

FEEDBACK CONTROL OF TWISTED STATES IN THE KURAMOTO MODEL ON NEAREST NEIGHBOR AND COMPLETE SIMPLE GRAPHS

KAZUYUKI YAGASAKI

ABSTRACT. We study feedback control of twisted states in the Kuramoto model (KM) of identical oscillators defined on deterministic nearest neighbor graphs containing complete simple ones when it may have phase-lag. Bifurcations of such twisted solutions in the continuum limit (CL) for the uncontrolled KM defined on nearest neighbor graphs that may be deterministic dense, random dense or random sparse were discussed very recently by using the center manifold reduction, which is a standard technique in dynamical systems theory. In this paper we analyze the stability and bifurcations of twisted solutions in the CL for the KM subjected to feedback control. In particular, it is shown that the twisted solutions exist and can be stabilized not only for nearest neighbor graphs but also for complete simple graphs. Moreover, the CL is shown to suffer bifurcations at which the twisted solutions becomes unstable and a stable one-parameter family of modulated or oscillating twisted solutions is born, depending on whether the phase-lag is zero or not. We demonstrate the theoretical results by numerical simulations for the feedback controlled KM on deterministic nearest neighbor and complete simple graphs.

1. INTRODUCTION

Coupled oscillators in complex networks have recently attracted significant attention and have been studied with rapidly increasing intensity [2, 5, 7, 18, 21, 24, 46, 47, 55, 57, 66, 74]. They provide many mathematical models in various fields such as physics, chemistry, biology, social sciences and engineering, and exhibit several collective dynamics including synchronization, chimeras and chaos. Among them, the Kuramoto model (KM) [33, 34] is one of the most representative models and has been generalized in several directions. It was originally proposed by Kuramoto [33, 34] half a century ago, and has continued to be the subject of enormous research, especially to discuss synchronization phenomena in diverse fields, since then. The range of its direct applications now spreads to power grids [15, 22, 27, 36, 38, 56, 58, 66], neuroscience [6, 8, 23, 52, 54, 55, 63, 72, 73], machine learning [3, 60, 65] and so on. See the above surveys and [1, 4, 6, 16, 52, 53, 62] for the reviews of vast literature on coupled oscillators in complex networks including the KM and its generalizations. The control problem of nonlinear oscillator networks is important not only in theoretical interest but also in applications, and has drawn much attention [13, 17, 48]. Feedback control of synchronized states different from twisted ones in the KM on

Date: January 6, 2026.

2020 Mathematics Subject Classification. 34C15; 34H05; 45J05; 34D06; 34C23; 37G10; 45M10; 34D20.

Key words and phrases. Kuramoto model; continuum limit; feedback control; twisted solution; bifurcation; center manifold reduction.

deterministic dense, random dense and random sparse graphs was studied numerically or theoretically in [17, 30, 32, 58, 59, 61, 71]. In particular, the stability of the target orbits was discussed theoretically only in [32, 71].

In this paper we consider feedback control of the KM consisting of identical oscillators on a deterministic dense graph $G_n = \langle V(G_n), E(G_n), W(G_n) \rangle$,

$$\begin{aligned} \frac{d}{dt}u_k^n(t) = & \omega + \frac{1}{n} \sum_{j=1}^n w_{kj}^n \sin(u_j^n(t) - u_k^n(t) + \sigma) \\ & + b_1(\hat{u}_k^n(t) - u_k^n(t)) + b_3(\hat{u}_k^n(t) - u_k^n(t))^3, \quad k \in [n] := \{1, 2, \dots, n\}, \end{aligned} \quad (1.1)$$

where $u_k^n : \mathbb{R} \rightarrow \mathbb{R}$ stands for the phase of oscillator at the node $k \in [n]$; $\hat{u}_k^n(t)$, $k \in [n]$, represent the target orbit; ω is the natural frequency; $\sigma \in (-\frac{1}{2}\pi, \frac{1}{2}\pi)$ is the phase-lag parameter; and $b_1, b_3 > 0$ are the linear and nonlinear feedback gains. We use the convenient notation $[n]$, which represents the set $\{1, 2, \dots, n\}$, throughout this paper. In [30, 32, 58, 59, 61, 68], a different nonlinear feedback control input,

$$\tilde{b}_1 \sin(V(t) - u_i^n(t)) + \tilde{b}_0,$$

where \tilde{b}_1, \tilde{b}_0 are constants with $\tilde{b}_1 > 0$, was treated.

On the other hand, $V(G_n) = [n]$ and $E(G_n)$ represent the sets of nodes and edges, respectively, and $W(G_n)$ is an $n \times n$ weight matrix given by

$$(W(G_n))_{kj} = \begin{cases} w_{kj}^n & \text{if } (k, j) \in E(G_n); \\ 0 & \text{otherwise.} \end{cases}$$

So we express

$$E(G_n) = \{(k, j) \in [n]^2 \mid (W(G_n))_{kj} \neq 0\},$$

where each edge is represented by an ordered pair of nodes (k, j) , which is also denoted by $j \rightarrow k$, and a loop is allowed. If $W(G_n)$ is symmetric, then G_n represents an undirected weighted graph and each edge is also denoted by $k \sim j$ instead of $j \rightarrow k$. When G_n is a simple graph, $W(G_n)$ is a matrix whose elements are $\{0, 1\}$ -valued. Moreover, the weight matrix $W(G_n)$ is assumed to be given as follows. Let $I = [0, 1]$ and let $W^n \in L^2(I^2)$, $n \in \mathbb{N}$, be nonnegative functions. We have

$$w_{kj}^n = \langle W^n \rangle_{kj}^n := n^2 \int_{I_k^n \times I_j^n} W^n(x, y) dx dy, \quad (1.2)$$

where

$$I_k^n := \begin{cases} [(k-1)/n, k/n] & \text{for } k < n; \\ [(n-1)/n, 1] & \text{for } k = n. \end{cases}$$

Such a function as $W^n(x, y)$ is usually called a *graphon* [39]. We also assume that there exists a measurable function $W \in L^2(I^2)$ such that

$$\|W(x, y) - W^n(x, y)\|_{L^2(I^2)} = \int_{I^2} |W(x, y) - W^n(x, y)|^2 dx dy \rightarrow 0 \quad (1.3)$$

as $n \rightarrow \infty$. We only assume here that G_n is deterministic, but can similarly treat the case in which it is random dense or sparse.

In [30], a general coupled oscillator network

$$\frac{d}{dt}u_k^n(t) = f(u_k^n(t), t) + \frac{1}{n} \sum_{l=1}^m \sum_{j=1}^n w_{kj}^{ln} D_l (u_j^n(t) - u_k^n(t)), \quad k \in [n], \quad (1.4)$$

defined on m (≥ 2) graphs G_{ln} , $l \in [m]$, which may be not only deterministic dense but also random dense or sparse, was studied and shown to be well approximated by the corresponding continuum limit (CL),

$$\frac{\partial}{\partial t} u(t, x) = f(u(t, x), t) + \sum_{l=1}^m \int_I W_l(x, y) D_l(u(t, y) - u(t, x)) dy, \quad x \in I, \quad (1.5)$$

where $u_k^n : \mathbb{R} \rightarrow \mathbb{R}$, $k \in [n]$, $f(u, t)$ is Lipschitz continuous in u and continuous in t and $D_l(u)$, $l \in [m]$, are bounded and Lipschitz continuous. The result is also applicable when the natural frequency at each node is different, and it was improved in [67], so that relationships between such a coupled oscillator network and its CL on the stability of their solutions were further developed. See Section 2 for more details on these results. Moreover, in [68], they were modified for the random natural frequency case by introducing a random permutation. Similar results for such networks defined on single graphs and having the same or equivalently zero, natural frequency at each node were obtained earlier in [31, 40, 41, 43] although neither the random natural frequencies nor stability of solutions were treated. Such a CL was introduced for the classical KM, which is defined on a single complete simple graph but may have natural frequencies depending on each oscillator, without a rigorous mathematical guarantee very early in [19], and it was fully discussed very recently in [67] when the natural frequencies are uniformly spaced. In [71] and [32], respectively, the results of [30, 67, 68] were used or extended successfully to discuss feedback control of the KM on uniform graphs which may be complete, random dense or sparse when the natural frequencies are uniformly spaced and random. Similar CLs were utilized for the KM with nonlocal coupling and a single or zero natural frequency in [25, 42, 45, 64]. However, the feedback controlled KM (1.1) does not have the form (1.4).

Here we take as the graphons $W^n(x, y)$ and $W(x, y)$

$$W^n(x, y) = \begin{cases} 1 & \text{if } (x, y) \in I_k^n \times I_j^n \text{ with } |k - j| \leq n\kappa \text{ or } |k - j| \geq n(1 - \kappa); \\ 0 & \text{otherwise,} \end{cases}$$

and

$$W(x, y) = \begin{cases} 1 & \text{if } |x - y| \leq \kappa \text{ or } |x - y| \geq 1 - \kappa; \\ 0 & \text{otherwise,} \end{cases}$$

with $0 < \kappa \leq \frac{1}{2}$, which correspond to nearest (more specifically, $\lfloor n\kappa \rfloor$ -nearest) neighbor graphs, where $\lfloor z \rfloor$ represents the maximum integer that is not greater than $z \in \mathbb{R}$. For $\kappa = \frac{1}{2}$, they become $W^n(x, y), W(x, y) \equiv 1$ and correspond to complete simple graphs. Moreover, we choose as the target orbit

$$\hat{u}_k^n(t) = \frac{2\pi qk}{n} + \Omega_D^n t, \quad k \in [n], \quad q \in \mathbb{N}, \quad (1.6)$$

where Ω_D^n is a constant given by

$$\Omega_D^n = \omega + \frac{1}{n} \sum_{|j| \leq n\kappa} \sin \left(\frac{2\pi qj}{n} + \sigma \right). \quad (1.7)$$

Note that Eq. (1.6) provides a particular solution to (1.1) even if $\kappa = \frac{1}{2}$, i.e., the graph G_n is complete simple, whether $b_1, b_3 = 0$ or not. Letting $v_k^n(t) =$

$u_k^n(t) - \hat{u}_k^n(t)$, $k \in [n]$, we rewrite (1.1) as

$$\begin{aligned} \frac{d}{dt}v_k^n(t) = & \omega + \frac{1}{n} \sum_{j=1}^n w_{kj}^n \cos \frac{2\pi q(j-k)}{n} \sin(v_j^n(t) - v_k^n(t) + \sigma) \\ & - \frac{1}{n} \sum_{j=1}^n w_{kj}^n \sin \frac{2\pi q(j-k)}{n} \cos(v_j^n(t) - v_k^n(t) + \sigma) \\ & - b_1 v_k^n(t) - b_3 v_k^n(t)^3, \quad k \in [n], \end{aligned} \quad (1.8)$$

which has the form (1.4). Using the results of [30, 67], we see that the coupled oscillator network (1.8) is well approximated by its CL

$$\begin{aligned} \frac{\partial}{\partial t}v(t, x) = & \omega + \int_I W(x, y) \cos 2\pi q(y - x) \sin(v(t, y) - v(t, x) + \sigma) dy \\ & - \int_I W(x, y) \sin 2\pi q(y - x) \cos(v(t, y) - v(t, x) + \sigma) dy, \\ & - b_1 v(x, t) - b_3 v(x, t)^3, \quad x \in I, \end{aligned} \quad (1.9)$$

so that the KM (1.1) is well approximated by the CL,

$$\begin{aligned} \frac{\partial}{\partial t}u(t, x) = & \omega + \int_I W(x, y) \sin(u(t, y) - u(t, x) + \sigma) dy \\ & + b_1(\hat{u}(t, x) - u(t, x)) + b_3(\hat{u}(t, x) - u(t, x))^3, \quad x \in I, \end{aligned} \quad (1.10)$$

where

$$\hat{u}(t, x) = 2\pi qx + \Omega t, \quad q \in \mathbb{N}, \quad (1.11)$$

and

$$\Omega = \omega + \int_{x-\kappa}^{x+\kappa} \sin(2\pi q(y - x) + \sigma) dy = \omega + \frac{\sin 2\pi q\kappa \sin \sigma}{\pi q}. \quad (1.12)$$

Note that Eq. (1.11) also provides a particular solution to (1.10), even if $\kappa = \frac{1}{2}$, i.e., $W(x, y) \equiv 1$, whether $b_1, b_3 = 0$ or not, although it is unstable for $\kappa = \frac{1}{2}$ and $b_1 = 0$ (see Remark 3.2(iii) below), and $\Omega = \lim_{n \rightarrow \infty} \Omega_D^n$. Moreover,

$$\left\| \hat{u}(t, x) - \sum_{i=1}^n \hat{u}_k^n(t) \mathbf{1}_{I_k^n} \right\|_{L^2(I)} = \int_I \left| \hat{u}(t, x) - \sum_{i=1}^n \hat{u}_k^n(t) \mathbf{1}_{I_k^n} \right|^2 dx \rightarrow 0$$

as $n \rightarrow \infty$, where $\mathbf{1}_{I_k^n}$ represents the characteristic function of I_k^n , $i \in [n]$.

In the previous work [70], the uncontrolled CL (1.10) with $b_1, b_3 = 0$ was studied and bifurcations of the q -twisted solutions

$$u(t, x) = 2\pi qx + \Omega t + \theta \in \mathbb{S}^1 := \mathbb{R}/2\pi\mathbb{Z}, \quad \theta \in \mathbb{S}^1, \quad q \in \mathbb{N}, \quad (1.13)$$

when κ is taken as a control parameter were analyzed by using the center manifold reduction [26, 29, 35], which is a standard technique in dynamical systems theory. In particular, it was shown in [70] that at the bifurcation points, the twisted solutions change their stability from stable to unstable, and stable or unstable modulated or oscillating twisted solutions are born, depending on whether $\sigma = 0$ or not, when κ is increased. The theoretical results for $q \in [2]$ or $[4]$ (recall that [2] and [4] represent the sets $\{1, 2\}$ and $\{1, 2, 3, 4\}$, respectively) were also demonstrated in numerical simulations for the uncontrolled KM (1.1) with $b_1, b_3 = 0$ defined on deterministic dense, random dense and random sparse nearest neighbor graphs although the observation of the modulated and oscillating twisted solutions born at

the bifurcations was impossible or very subtle since they are unstable or considered to disappear near the bifurcations. A similar bifurcation analysis was performed for synchronized solutions in the CL of the KM with two-mode interaction defined on two graphs in [69].

Here we take the linear feedback gain b_1 as a control parameter and analyze bifurcations of the q -twisted solution (1.11) in the controlled CL (1.10) with $b_1, b_3 \neq 0$ for $q \in [4]$, using the center manifold reduction as in [69, 70]. We show that at the bifurcation points, the twisted solutions change their stability from stable to unstable, and stable modulated or oscillating twisted solutions depending on whether $\sigma = 0$ or not, when b_1 is decreased and $b_3 > 0$ is sufficiently large. This is similar to the uncontrolled case of $b_1, b_3 = 0$, but a little different since modulated and oscillating twisted solutions born at the bifurcations are stable in a wide range of the control parameter b_1 . The CL (1.10) can be controlled to exhibit the desired q -twisted solution (1.11), which is the same as (1.13) with $\theta = 0$, for $q \in [4]$, by choosing appropriate values of b_1, b_3 , even if the one-parameter family (1.13) of q -twisted solutions is unstable when $b_1, b_3 = 0$. Moreover, the modulated twisted solutions, which are unstable in the uncontrolled case of $b_1, b_3 = 0$ for $q \in [4]$, are also stabilized by the feedback control when taking a sufficiently large value of $b_3 > 0$. It follows from the results of [30, 67] that such bifurcations are also expected to occur in the KM (1.1) (see Remarks 4.3(iii) and 4.5(iii) below). In particular, if the q -twisted solution (1.11) is asymptotically stable in the CL (1.10), then our feedback control is considered to be successful since the q -twisted state (1.6) is expected to be asymptotically stable in the KM (1.1). We demonstrate our theoretical results by numerical simulations for the KM (1.1) on deterministic nearest neighbor and complete simple graphs. Stable modulated and oscillating twisted states are observed clearly in wide ranges of b_1 in the numerical simulations.

The outline of this paper is as follows: In Section 2 we briefly review the previous fundamental results of [30, 67] on relationships between coupled oscillators and their CLs in the context of (1.1) and (1.10). In particular, we will see that an asymptotically stable and unstable solutions to the CL (1.10), respectively, behave as if they are asymptotically stable and unstable in the KM (1.1). We analyze the associated linear eigenvalue problem for q -twisted solutions to the CL (1.10) in Section 3, and discuss their bifurcations for $q \in [4]$ in Section 4. Numerical simulation results of the KM (1.1) on the nearest neighbor and complete simple graphs are given in Sections 5 and 6, respectively.

2. RELATIONSHIPS BETWEEN THE KM (1.1) AND CL (1.10)

We first review the results of [30, 67] on relationships between coupled oscillator networks and their CLs in the context of the KM (1.1) and CL (1.10). See Section 2 and Appendices A and B of [30] and Section 2 of [67] for more details, including the proofs of the theorems stated below. These results for (1.1) and (1.10) follow from application of the results of [30, 67] to (1.8) and (1.9).

Let $g(x) \in L^2(I)$ and let $\mathbf{u} : \mathbb{R} \rightarrow L^2(I)$ stand for an $L^2(I)$ -valued function. We have the following on the existence and uniqueness of solutions to the initial value problem (IVP) of the CL (1.10) (see Theorem 2.1 of [30]).

Theorem 2.1. *There exists a unique solution $\mathbf{u}(t) \in C^1(\mathbb{R}, L^2(I))$ to the IVP of (1.10) with*

$$u(0, x) = g(x).$$

Moreover, the solution depends continuously on g .

We next consider the IVP of the KM (1.1) and turn to the issue on convergence of solutions in (1.1) to those in the CL (1.10). Since the right-hand side of (1.1) is Lipschitz continuous in u_k^n , $i \in [n]$, we see by a fundamental result of ordinary differential equations (e.g., Theorem 2.1 of Chapter 1 of [12]) that the IVP of (1.1) has a unique solution. Given a solution $u_n(t) = (u_1^n(t), \dots, u_n^n(t))$ to the IVP of (1.1), we define an $L^2(I)$ -valued function $\mathbf{u}_n : \mathbb{R} \rightarrow L^2(I)$ as

$$\mathbf{u}_n(t) = \sum_{i=1}^n u_k^n(t) \mathbf{1}_{I_k^n}.$$

Recall that $\mathbf{1}_{I_k^n}$ represents the characteristic function of I_k^n , $i \in [n]$. Let $\|\cdot\|$ denote the norm in $L^2(I)$. In our setting stated in Section 1, we slightly modify the arguments given in the proof of Theorem 2.3 of [30] to obtain the following (see also Theorem 2.2 of [67]).

Theorem 2.2. *If $\mathbf{u}_n(t)$ is the solution to the IVP of (1.1) with the initial condition*

$$\lim_{n \rightarrow \infty} \|\mathbf{u}_n(0) - \mathbf{u}(0)\| = 0,$$

then for any $T > 0$ we have

$$\lim_{n \rightarrow \infty} \max_{t \in [0, T]} \|\mathbf{u}_n(t) - \mathbf{u}(t)\| = 0,$$

where $\mathbf{u}(t)$ represents the solution to the IVP of the CL (1.10).

We also obtain the following result, slightly modifying the proof of Theorem 2.5 in [30] (see also Theorem 2.3 of [67]).

Theorem 2.3. *Suppose that the KM (1.1) and CL (1.10) have solutions $\bar{\mathbf{u}}_n(t)$ and $\bar{\mathbf{u}}(t)$, respectively, such that*

$$\lim_{n \rightarrow \infty} \|\bar{\mathbf{u}}_n(t) - \bar{\mathbf{u}}(t)\| = 0 \tag{2.1}$$

for any $t \in [0, \infty)$. Then the following hold:

(i) *If for any $\varepsilon > 0$, there exist $\delta_1 > 0$ such that for $n > 0$ sufficiently large, any solution $\bar{u}_i^n(t)$, $i \in [n]$, to the KM (1.1) with*

$$|u_i^n(0) - \bar{u}_i^n(0)| < \delta_1, \quad i \in [n],$$

satisfies

$$|u_i^n(t) - \bar{u}_i^n(t)| < \varepsilon, \quad i \in [n],$$

then $\bar{\mathbf{u}}(t)$ is stable. Moreover, If for any $\varepsilon > 0$, there exists $\delta_2 > 0$ such that for $n > 0$ sufficiently large, any solution $\bar{u}_i^n(t)$, $i \in [n]$, to the KM (1.1) with

$$|u_i^n(t) - \bar{u}_i^n(t) - \theta| < \delta_2, \quad i \in [n],$$

converges to $\bar{u}_i^n(t)$, $i \in [n]$, then $\bar{\mathbf{u}}(t)$ is asymptotically stable.

(ii) *If $\bar{\mathbf{u}}(t)$ is stable, then for any $\varepsilon, T > 0$ there exists $\delta > 0$ such that for $n > 0$ sufficiently large, if $\bar{\mathbf{u}}_n(t)$ is a solution to the KM (1.1) satisfying*

$$\|\mathbf{u}_n(0) - \bar{\mathbf{u}}_n(0)\| < \delta,$$

then

$$\|\mathbf{u}_n(t) - \bar{\mathbf{u}}_n(t)\| < \varepsilon.$$

Moreover, if $\bar{\mathbf{u}}(t)$ is asymptotically stable, then

$$\lim_{t \rightarrow \infty} \lim_{n \rightarrow \infty} \|\mathbf{u}_n(t) - \bar{\mathbf{u}}(t)\| = 0,$$

where $\mathbf{u}_n(t)$ is any solution to (1.1) such that $\mathbf{u}_n(0)$ is contained in the basin of attraction for $\bar{\mathbf{u}}(t)$.

Remark 2.4.

- (i) The solution $\bar{\mathbf{u}}_n(t)$ may not be asymptotically stable in the KM (1.1) for $n > 0$ sufficiently large even if so is $\bar{\mathbf{u}}(t)$ in the CL (1.10). In the definition of stability and asymptotic stability of solutions to the CL (1.10), we cannot distinguish two solutions that are different only in a set with the Lebesgue measure zero.
- (ii) From the proof of Theorem 2.5 in [30] the stability stated in Theorem 2.3 contains not only the Lyapunov meaning but also the orbital one.

We have the following as a corollary of Theorem 2.3, without assuming the existence of the solution $\bar{\mathbf{u}}_n(t)$ to the KM (1.1) satisfying (2.1) (see the proof of Theorem 2.4(ii) and Corollary 2.6 of [67]).

Corollary 2.5. Suppose that the CL (1.10) has a stable solution $\bar{\mathbf{u}}(t)$. Then for any $\varepsilon, T > 0$ there exists $\delta > 0$ such that for $n > 0$ sufficiently large, if $\mathbf{u}_n(t)$ is a solution to the KM (1.1) satisfying

$$\|\mathbf{u}_n(0) - \bar{\mathbf{u}}(0)\| < \delta,$$

then

$$\max_{t \in [0, T]} \|\mathbf{u}_n(t) - \bar{\mathbf{u}}(t)\| < \varepsilon.$$

Moreover, if $\bar{\mathbf{u}}(t)$ is asymptotically stable, then

$$\lim_{t \rightarrow \infty} \lim_{n \rightarrow \infty} \|\mathbf{u}_n(t) - \bar{\mathbf{u}}(t)\| = 0,$$

where $\mathbf{u}_n(t)$ is any solution to (1.1) such that $\mathbf{u}_n(0)$ is contained in the basin of attraction for $\bar{\mathbf{u}}(t)$.

Remark 2.6.

- (i) In Corollary 2.6 of [67] only complete simple graphs were treated but Corollary 2.5 can be proven similarly since its proof relies only on Theorem 2.2 of [67], of which extension to (1.1) and (1.10) is Theorem 2.2.
- (ii) Corollary 2.5 implies that $\bar{\mathbf{u}}(t)$ behaves as if it is an (asymptotically) stable family of solutions in the KM (1.1).

Finally, modifying the arguments given in the proofs of Theorems 2.7 and 2.9 of [67] slightly, we obtain the following results.

Theorem 2.7. Suppose that the hypothesis of Theorem 2.3 holds. Then the following hold:

- (i) If $\bar{\mathbf{u}}_n(t)$ is unstable for $n > 0$ sufficiently large and no stable solution to the KM (1.1) converges to $\bar{\mathbf{u}}(t)$ as $n \rightarrow \infty$, then $\bar{\mathbf{u}}(t)$ is unstable.
- (ii) If $\bar{\mathbf{u}}(t)$ is unstable, then so is $\bar{\mathbf{u}}_n(t)$ for $n > 0$ sufficiently large.

Theorem 2.8. If $\bar{\mathbf{u}}(t)$ is unstable, then for any $\varepsilon, \delta > 0$ there exists $T > 0$ such that for $n > 0$ sufficiently large

$$\max_{t \in [0, T]} \|\mathbf{u}_n(t) - \bar{\mathbf{u}}(t)\| > \varepsilon,$$

where $\mathbf{u}_n(t)$ is a solution to the KM (1.1) satisfying

$$\|\mathbf{u}_n(0) - \bar{\mathbf{u}}(0)\| < \delta.$$

Remark 2.9.

- (i) Only under the hypothesis of Corollary 2.5, $\mathbf{u}(t)$ is not necessarily unstable even if $\mathbf{u}_n(t)$ is unstable for $n > 0$ sufficiently large. Moreover, $\mathbf{u}(t)$ may be asymptotically stable even if $\mathbf{u}_n(t)$ is unstable for $n > 0$ sufficiently large. See [67] for such an example.
- (ii) In Theorem 2.9 of [67] only complete simple graphs were treated but Theorem 2.8 can be proven similarly, like Corollary 2.5, as stated in Remark 2.6(i).
- (iii) Theorem 2.8 implies that $\bar{\mathbf{u}}(t)$ behaves as if it is an unstable family of solutions in the KM (1.1).

Thus, the relationship between the KM (1.1) and CL (1.10) is subtle. However, under the hypothesis of Corollary 2.5, if $\bar{\mathbf{u}}(t)$ is asymptotically stable, then a solution to the KM (1.1) starting in the basin of attraction of $\bar{\mathbf{u}}(t)$ stays near $\bar{\mathbf{u}}(t)$ for $n, t > 0$ sufficiently large. This conclusion indicates that the “asymptotic stability” of $\mathbf{u}_n(t)$ is observed in numerical simulations since they can be performed only for large finite values of $n, t > 0$. We will observe this behavior in numerical simulations in Sections 5 and 6.

3. LINEAR STABILITY

We now return to the CL (1.10) and first determine the linear stability of the solution (1.11) to the CL (1.10). Following the approach of Section 3 in [70], we consider the eigenvalue problem for the linear operator $\mathcal{L} : L^2(I) \rightarrow L^2(I)$ given by

$$\begin{aligned} \mathcal{L}\phi(x) &= \int_I W(x, y) \cos(2\pi q(y - x) + \sigma)(\phi(y) - \phi(x)) dy - b\phi(x) \\ &= \int_{x-\kappa}^{x+\kappa} \cos(2\pi q(y - x) + \sigma)\phi(y) dy - \left(\frac{\cos \sigma \sin 2\pi q\kappa}{\pi q} + b_1 \right) \phi(x) \end{aligned}$$

for the linearization of (1.10) around $u(t, x) = 2\pi qx$.

Obviously, $\phi(x) = 1$ is an eigenfunction for the eigenvalue $\lambda = -b_1 < 0$. Moreover, if $\sigma = 0$, then

$$\phi(x) = \cos 2\pi \ell x, \sin 2\pi \ell x$$

are eigenfunctions for the eigenvalue

$$\lambda = \chi_1(\ell, q) - b_1$$

for each $\ell \in \mathbb{N}$, and if $\sigma \neq 0$, then

$$\phi(x) = \cos 2\pi \ell x \pm i \sin 2\pi \ell x$$

are eigenfunctions for the eigenvalue

$$\lambda = \chi_1(\ell, q) \cos \sigma - b_1 \mp i \chi_2(\ell, q) \sin \sigma$$

for each $\ell \in \mathbb{N}$, where the upper or lower signs are taken simultaneously,

$$\chi_1(\ell, q) = \begin{cases} \kappa + \frac{\sin 4\pi q\kappa}{4\pi q} - \frac{\sin 2\pi q\kappa}{\pi q} & \text{if } \ell = q; \\ \frac{\sin 2\pi(\ell - q)\kappa}{2\pi(\ell - q)} + \frac{\sin 2\pi(\ell + q)\kappa}{2\pi(\ell + q)} - \frac{\sin 2\pi q\kappa}{\pi q} & \text{otherwise} \end{cases}$$

and

$$\chi_2(\ell, q) = \begin{cases} \kappa - \frac{\sin 4\pi q \kappa}{4\pi q} & \text{if } \ell = q; \\ \frac{\sin 2\pi(\ell - q)\kappa}{2\pi(\ell - q)} - \frac{\sin 2\pi(\ell + q)\kappa}{2\pi(\ell + q)} & \text{otherwise.} \end{cases}$$

See also Section 3 of [70]. These eigenvalues are the only ones of \mathcal{L} since the Fourier expansion of any function in $L^2(I)$ converges a.e. by Carleson's theorem [10]. Thus, if

$$b_1 > \chi_1(\ell, q) \cos \sigma \quad (3.1)$$

for any $\ell \in \mathbb{N}$, then the q -twisted solution (1.11) is linearly stable. In addition, if

$$b_1 = \chi_1(\ell, q) \cos \sigma \quad (3.2)$$

then \mathcal{L} has a zero eigenvalue of geometric multiplicity two when $\sigma = 0$ and a pair of purely imaginary eigenvalues when $\sigma \neq 0$ and $\chi_2(\ell, q) \neq 0$, so that a bifurcation may occur in the CL (1.10).

Let

$$\varphi(\zeta) = \frac{2 \sin \zeta}{\zeta} - \frac{\sin 2\zeta}{2\zeta} = \frac{\sin \zeta}{\zeta} (2 - \cos \zeta).$$

We show that the equation $\varphi(\zeta) = 1$ has a unique root at

$$\zeta_0 = 2.1391 \dots$$

in $(0, \pi)$ (see Section 3 of [70]). The following properties on $\chi_1(\ell, q)$ hold, as proven in Proposition 3.2 of [70].

Proposition 3.1.

- (i) $\chi_1(q, q) = \frac{1}{2}$ and $\chi_1(\ell, q) = 0$ for $\ell \neq q$ at $\kappa = \frac{1}{2}$, while $\chi_1(\ell, q) \rightarrow 0$ as $\kappa \rightarrow +0$ for any $\ell \in \mathbb{N}$.
- (ii) $\chi_1(q, q) < 0$ for $\kappa \in (0, \kappa_q)$ and $\chi_1(q, q) > 0$ for $\kappa \in (\kappa_q, \frac{1}{2})$, where $\kappa_q = \zeta_0/2\pi q$.
- (iii) For any $\ell \in \mathbb{N}$, $\chi_1(\ell, q) < 0$ when $\kappa > 0$ is sufficiently small.
- (iv) If $\ell \geq 2q$ and $\kappa \leq \kappa_q$, then $\chi_1(\ell, q) < \chi_1(q, q)$.

Remark 3.2.

- (i) From Proposition 3.1(i) we see that for each $q \in \mathbb{N}$, the q -twisted solution (1.11) is linearly stable if $b_1 > \chi_1(\kappa; q, q)$, near $\kappa = \frac{1}{2}$, and especially at $\kappa = \frac{1}{2}$, i.e., when the graph G_n is complete simple.
- (ii) It follows from Proposition 3.1(ii)-(iv) that for $q \in \mathbb{N}$ the q -twisted solution (1.11) is asymptotically stable for $b_1 > 0$ when $\kappa > 0$ is sufficiently small or when $\kappa < \kappa_q$ and $\chi_1(\kappa; \ell, q) < 0$ for $\ell < 2q$.
- (iii) When $b_1 = 0$ and $\kappa = \frac{1}{2}$, the q -twisted solution (1.11) is unstable for any $q \in \mathbb{N}$, by Proposition 3.1(i).

Figure 1 displays the dependence of $\chi_1(\ell, q)$ on κ for $q \in [4]$ and some values of ℓ . If we choose such a sufficient large value of b_1 that Eq. (3.1) holds, i.e., $\chi_1(\ell, q) < b_1$, for all $\ell \in \mathbb{N}$, then q -twisted solution (1.11) is asymptotically stable. In particular, we can stabilize the q -twisted solution (1.11) for complete simple graphs. We also observe that $\chi_1(q, q) \rightarrow \frac{1}{2}$ and $\chi_1(\ell, q) \rightarrow 0$ for $\ell \neq q$ as $\kappa \rightarrow \frac{1}{2} - 0$ while $\chi_1(\ell, q) < 0$ near $\kappa = 0$, as stated in Proposition 3.1(i) and (iii). For $q \in [4]$, the q -twisted solution (1.11) is asymptotically stable if $b_1 > 0$ and $\kappa < \kappa_q$, by

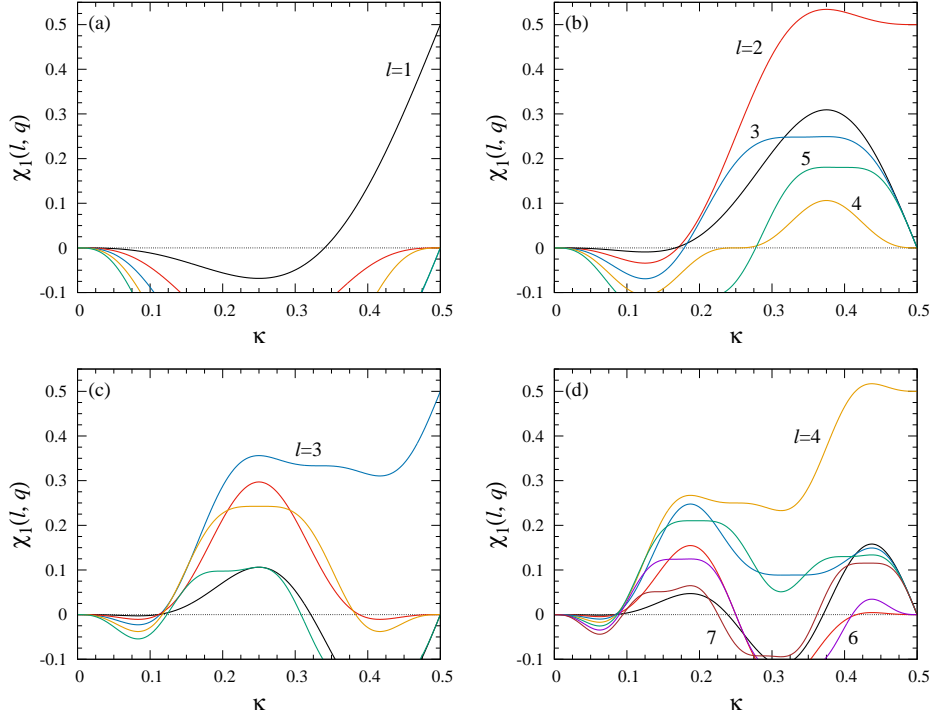


FIGURE 1. Dependence of $\chi_1(l, q)$ on κ for $l = 1-7$: (a) $q = 1$; (b) $q = 2$; (c) $q = 3$; (d) $q = 4$. It is plotted as the line of which color is black for $l = 1$, red for $l = 2$, blue for $l = 3$, orange for $l = 4$, green for $l = 5$, purple for $l = 6$ and brown for $l = 7$.

Remark 3.2(ii). Moreover, $\chi_1(q, q) > \chi_1(\ell, q)$ in wide ranges of κ for $q \in [4]$. In particular, $\chi_1(1, 1) > \chi_1(\ell, 1)$ on $\kappa \in (0, \frac{1}{2})$ for any $\ell > 1$, by Proposition 3.1(iv).

Since $\chi_2(q, q)$ is monotonically increasing as a function of κ on $(0, \frac{1}{2}]$, we easily prove the following.

Proposition 3.3. $\chi_1(q, q) \rightarrow 0$ as $\kappa \rightarrow +0$, $\chi_2(q, q) = \frac{1}{2}$ at $\kappa = \frac{1}{2}$, and $\chi_2(q, q) > 0$ for $\kappa \in (0, \frac{1}{2}]$.

4. BIFURCATIONS

We now take the linear feedback gain b_1 as a control parameter and analyze bifurcations of the q -twisted solution (1.11) in the CL (1.10) for $q \in [4]$. Our approach is similar to that of [70] for the uncontrolled case of $b_1, b_3 = 0$ but some modifications are required.

Let b_{1q} denote the value of b_1 satisfying (3.2) for $\ell = q$, i.e.,

$$b_{1q} = \chi_1(q, q) \cos \sigma. \quad (4.1)$$

From the analysis of Section 3 we see that a bifurcation may occur at $b_1 = b_{1q}$ for each $q \in \mathbb{N}$. In the following we analyze the bifurcation which may occur at (4.1) for $q \in [4]$. We assume for each $q \in [4]$ that $b_1 \approx b_{1q}$ and condition (3.1) holds for $\ell \neq q$, and introduce a parameter $\mu = b_1 - b_{1q} \approx 0$. Moreover, we write solutions

to the CL (1.10) near the q -twisted solution (1.11) as

$$u(t, x) = 2\pi qx + \Omega t + \xi_0(t) + \sum_{j=1}^{\infty} (\xi_j(t) \cos 2\pi jx + \eta_j(t) \sin 2\pi jx) \quad (4.2)$$

and regard μ as a state variable.

4.1. Center manifold reduction. We substitute (4.2) into (1.10) and integrate the resulting equation from $x = 0$ to 1 directly or after multiplying it with $\cos 2\pi jx$ or $\sin 2\pi jx$, $j \in \mathbb{N}$, to obtain

$$\begin{aligned} \dot{\xi}_q &= -\mu \xi_q - \nu_q \eta_q - \left(\frac{3}{4}b_3 + \beta_1 \cos \sigma\right)(\xi_q^2 + \eta_q^2) \xi_q + \delta_1 \cos \sigma (\xi_q \eta_{2q} - \xi_{2q} \eta_q) \\ &\quad + \sin \sigma (-\beta_2 (\xi_q^2 + \eta_q^2) \eta_q + \delta_2 (\xi_q \xi_{2q} + \eta_q \eta_{2q})) + \dots, \\ \dot{\eta}_q &= \nu_q \xi_q - \mu \eta_q - \left(\frac{3}{4}b_3 + \beta_1 \cos \sigma\right)(\xi_q^2 + \eta_q^2) \eta_q - \delta_1 \cos \sigma (\xi_q \xi_{2q} + \eta_q \eta_{2q}) \\ &\quad + \sin \sigma (\beta_2 (\xi_q^2 + \eta_q^2) \xi_q + \delta_2 (\xi_q \eta_{2q} - \xi_{2q} \eta_q)) + \dots, \\ \dot{\xi}_{2q} &= \mu_{2q} \xi_{2q} - \nu_{2q} \eta_{2q} - 2\rho_1 \xi_q \eta_q \cos \sigma + \rho_2 \sin \sigma (\xi_q^2 - \eta_q^2) + \dots, \\ \dot{\eta}_{2q} &= \nu_{2q} \xi_{2q} + \mu_{2q} \eta_{2q} + \rho_1 \cos \sigma (\xi_q^2 - \eta_q^2) + 2\rho_2 \xi_q \eta_q \sin \sigma + \dots, \\ \dot{\xi}_j &= \mu_j \xi_j - \nu_j \eta_j + \dots, \quad \dot{\eta}_j = \nu_j \xi_j + \mu_j \eta_j + \dots, \quad j \in \mathbb{N} \setminus \{q, 2q\} \\ \dot{\xi}_0 &= -b_{1q} \xi_0 + \dots, \quad \dot{\mu} = 0, \end{aligned} \quad (4.3)$$

for $q \in [4]$, where ‘ \dots ’ represents higher-order terms of

$$O\left(\xi_q^4 + \eta_q^4 + \xi_0^2 + \sum_{j=1, j \neq q}^{\infty} (\xi_j^2 + \eta_j^2) + \mu^2\right)$$

for the first and second equations and

$$O\left(\xi_0^2 + \sum_{j=1}^{\infty} (\xi_j^2 + \eta_j^2) + \mu^2\right)$$

for the other equations, and

$$\begin{aligned} \beta_1 &= \frac{3}{8}a_2(q, 0) - \frac{1}{2}a_2(q, q) + \frac{1}{8}a_2(q, 2q), \quad \beta_2 = \frac{1}{4}a_1(q, q) - \frac{1}{8}a_1(q, 2q), \\ \delta_1 &= a_1(q, q) - \frac{1}{2}a_1(q, 2q), \quad \delta_2 = \frac{1}{2}a_2(q, 0) - \frac{1}{2}a_2(q, 2q), \\ \rho_1 &= \frac{1}{2}a_1(q, q) - \frac{1}{4}a_1(q, 2q), \quad \rho_2 = \frac{1}{4}a_2(q, 0) - \frac{1}{2}a_2(q, q) + \frac{1}{4}a_2(q, 2q), \\ \mu_j &= -b_{1q} + \chi_1(j, q) \cos \sigma, \quad j \in \mathbb{N} \setminus \{1\}, \\ \nu_j &= \chi_2(j, q) \sin \sigma, \quad j \in \mathbb{N}, \end{aligned}$$

with

$$\begin{aligned} a_1(q, j) &= \begin{cases} \frac{\sin(4\pi q\kappa)}{4\pi q} - \kappa & \text{for } j = q; \\ \frac{q \sin(2\pi j\kappa) \cos(2\pi q\kappa) - j \cos(2\pi j\kappa) \sin(2\pi q\kappa)}{\pi(q^2 - j^2)} & \text{for } j \neq q, \end{cases} \\ a_2(q, j) &= \begin{cases} -\frac{\sin 4\pi q\kappa}{4\pi q} - \kappa & \text{for } j = q; \\ \frac{j \sin(2\pi j\kappa) \cos(2\pi q\kappa) - q \cos(2\pi j\kappa) \sin(2\pi q\kappa)}{\pi(q^2 - j^2)} & \text{for } j \neq q. \end{cases} \end{aligned}$$

See Appendix A for the derivation of (4.3).

Henceforth we assume that $\mu_j < 0$ for any $j \neq q \in [4]$. Actually, this assumption holds near $\kappa = \frac{1}{2}$ by Remark 3.2(i), and in a wide range of κ containing $(0, \kappa_q]$ as seen from Fig. 1 and Proposition 3.1(iv). The origin in the infinite-dimensional system (4.3) is an equilibrium having a three-dimensional center manifold W^c , even if $\sigma \neq 0$. Using the standard approach [26, 29, 35], we obtain the following.

Proposition 4.1. *The center manifold is expressed as*

$$W^c = \{\xi_{2q} = \bar{\xi}_{2q}(\xi_q, \eta_q) + O(3), \eta_{2q} = \bar{\eta}_{2q}(\xi_q, \eta_q) + O(3), \\ \xi_0 = O(3), \xi_j = O(3), \eta_j = O(3), j \neq q, 2q\}$$

near the origin, where $O(k)$ represents higher-order terms of $O\left(\sqrt{\xi_q^{2k} + \eta_q^{2k} + \mu^4}\right)$, and

$$\bar{\xi}_{2q}(\xi_q, \eta_q) = c_1(\xi_q^2 - \eta_q^2) + 2c_2\xi_q\eta_q, \quad \bar{\eta}_{2q}(\xi_q, \eta_q) = -c_2(\xi_q^2 - \eta_q^2) + 2c_1\xi_q\eta_q$$

with

$$c_1 = \frac{(2\nu_q - \nu_{2q})\rho_1 \cos \sigma - \mu_{2q}\rho_2 \sin \sigma}{\mu_{2q}^2 + (2\nu_q - \nu_{2q})^2}, \\ c_2 = \frac{\mu_{2q}\rho_1 \cos \sigma - (2\nu_q - \nu_{2q})\rho_2 \sin \sigma}{\mu_{2q}^2 + (2\nu_q - \nu_{2q})^2}.$$

Based on Proposition 4.1, we apply the center manifold reduction [29] to (4.3). and obtain

$$\begin{aligned} \dot{\xi}_q &= -\mu\xi_q - \nu_q\eta_q \\ &\quad - \left(\frac{3}{4}b_3 + \beta_1 \cos \sigma\right)(\xi_q^2 + \eta_q^2)\xi_q + \delta_1 \cos \sigma(\bar{\eta}_{2q}(\xi_q, \eta_q)\xi_q - \bar{\xi}_{2q}(\xi_q, \eta_q)\eta_q) \\ &\quad + \sin \sigma(-\beta_2(\xi_q^2 + \eta_q^2)\eta_q + \delta_2(\bar{\xi}_{2q}(\xi_q, \eta_q)\xi_q + \bar{\eta}_{2q}(\xi_q, \eta_q)\eta_q)) + O(4), \\ \dot{\eta}_q &= \nu_q\xi_q - \mu\eta_q \\ &\quad - \left(\frac{3}{4}b_3 + \beta_1 \cos \sigma\right)(\xi_q^2 + \eta_q^2)\eta_q + \delta_1 \cos \sigma(\bar{\xi}_{2q}(\xi_q, \eta_q)\xi_q + \bar{\eta}_{2q}(\xi_q, \eta_q)\eta_q) \\ &\quad + \sin \sigma(\beta_2(\xi_q^2 + \eta_q^2)\xi_q + \delta_2(\bar{\eta}_{2q}(\xi_q, \eta_q)\xi_q - \bar{\xi}_{2q}(\xi_q, \eta_q)\eta_q)) + O(4), \\ \dot{\mu} &= 0 \end{aligned} \tag{4.4}$$

on W^c . See Appendix B of [69] for the validity of application of the center manifold theory on infinite-dimensional dynamical systems [29]. The origin $(\xi_q, \eta_q, \mu) = (0, 0, 0)$ is always an equilibrium in (4.4). This is because the twisted solution (1.11) necessarily satisfies the CL (1.10).

4.2. Case of $\sigma = 0$. We set $\sigma = 0$, so that $c_1 = 0$ and $c_2 = -\rho_1/\mu_{2q}$. We remark that

$$\mu_{2q} = -b_{1q} + \chi_1(2q, q) = -\kappa + \frac{\sin 2\pi q \kappa}{2\pi q} < 0$$

for $\kappa > 0$. Letting $r = \sqrt{\xi_q^2 + \eta_q^2} \geq 0$, we rewrite (4.4) as

$$\dot{r} = -\mu r - \beta_0 r^3 + O(\sqrt{r^8 + \mu^4}), \quad \dot{\mu} = 0, \tag{4.5}$$

where

$$\beta_0 = \frac{3}{4}b_3 + \bar{\beta}_1, \quad \bar{\beta}_1 = \beta_1 + \frac{\delta_1 \rho_1}{\mu_{2q}}. \tag{4.6}$$

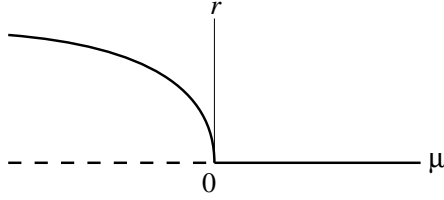


FIGURE 2. Bifurcation diagrams for (4.5).

In particular, $\bar{\beta}_1 = 0$ when $\kappa = \frac{1}{2}$. Here by the translation symmetry, the first equation of (4.5) must depend only on r and μ , even if the higher-order terms are included. We take such a sufficiently large value for b_3 as $\beta_0 > 0$. We easily show the following for (4.5):

- (i) The equilibrium $r = 0$ is stable for $\mu > 0$ and unstable for $\mu < 0$;
- (ii) There exists another stable equilibrium at

$$r = \sqrt{-\frac{\mu}{\beta_0}}$$

for $\mu < 0$.

See Fig. 2 for the bifurcation diagrams for (4.5). From this result, we obtain the following for the CL (1.10).

Theorem 4.2. *Let $q \in [4]$ and suppose that $\beta_0 > 0$, i.e., $b_3 > -\frac{4}{3}\bar{\beta}_1$, and $\mu_j = -b_{1q} + \chi_1(j, q) < 0$ for any $j \neq q$. Then the following bifurcation of the twisted solution (1.11) occurs at $b_1 = b_{1q}$ in the CL (1.10) with $\sigma = 0$:*

- (i) *The twisted solution (1.11) is stable for $b_1 > b_{1q}$ and unstable for $b_1 < b_{1q}$;*
- (ii) *There exists a stable one-parameter family of modulated twisted solutions*

$$\mathcal{U}^q = \left\{ u = 2\pi q x + \sqrt{-\frac{b_1 - b_{1q}}{\beta_0}} \sin(2\pi q x + \psi) + \omega t + O(b_1 - b_{1q}) \middle| \psi \in \mathbb{S}^1 \right\} \quad (4.7)$$

for $b_1 < b_{1q}$ near $b_1 = b_{1q}$, where $\beta_0 = O(1)$ is given in (4.6).

Remark 4.3.

- (i) *A bifurcation similar to one detected in Theorem 4.2 also occurs at $b_1 = b_{1q}$ even if $b_3 < -\frac{4}{3}\bar{\beta}_1$ or $\mu_j > 0$ for some $j \neq q$, although the one-parameter family \mathcal{U}^q of modulated twisted solutions born there is unstable.*
- (ii) *We suspect for any $q \in \mathbb{N}$ that Eq. (4.3) is valid and the statements of Theorem 4.2 also hold. However, it is very hard to derive (4.3) for any $q \in \mathbb{N}$, so that we restrict ourselves to $q \in [4]$ in the above analysis.*
- (iii) *From Corollary 2.5 and Theorem 2.8 we see that the twisted solution (1.11) (resp. \mathcal{U}^q) behaves as if it is an asymptotically stable or unstable solution (resp. a asymptotically stable families of solutions) in the KM (1.1) near $b_1 = b_{1q}$ for $n > 0$ sufficiently large, as stated in Remarks 2.6(ii) and 2.9(ii). Thus, the KM (1.1) suffers a “bifurcation” similar to one detected in Theorem 4.2 for the CL (1.10).*

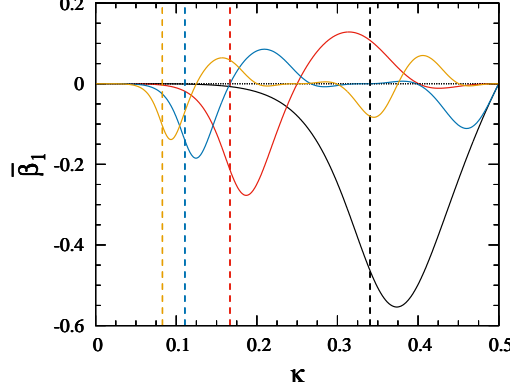


FIGURE 3. Dependence of $\bar{\beta}_1$ on κ . The black, red, blue and orange lines represent the cases of $q = 1, 2, 3$ and 4 , respectively. The dashed lines with the same colors represent $\kappa = \kappa_q$, on which $b_{1q} = 0$, for $q \in [4]$.

Figure 3 displays the dependence of $\bar{\beta}_1$ given by (4.6) on κ for $q \in [4]$. In particular, $\bar{\beta}_1 = 0$ at $\kappa = \frac{1}{2}$. Theorem 4.2 requires $b_3 > -\frac{4}{3}\bar{\beta}_1$ and $b_{1q} = \chi_1(q, q) > \chi_1(j, q)$ for any $j \neq q$ as its hypotheses. The nonlinear feedback gain b_3 has to be positive at least for the former to hold in the range of κ where $\bar{\beta}_1$ is negative, especially near $\kappa = \frac{1}{2}$ and for $q = 1$. From Fig. 1 and Proposition 3.1(iv) we see that the latter holds for $q \in [4]$ when $\kappa \leq \kappa_q$.

4.3. Case of $\sigma \neq 0$. We next consider the case of $\sigma \neq 0$. Letting $\xi_q = r \cos \psi$ and $\eta_q = r \sin \psi$, we rewrite (4.4) as

$$\dot{r} = -\mu r - \beta_\sigma r^3 + O(\sqrt{r^8 + \mu^4}), \quad \dot{\psi} = \nu_q + O(\sqrt{r^2 + \mu^2}), \quad \dot{\mu} = 0, \quad (4.8)$$

where

$$\beta_\sigma = \frac{3}{4}b_3 + \bar{\beta}_{1\sigma} \quad (4.9)$$

with

$$\begin{aligned} \bar{\beta}_{1\sigma} = & \beta_1 \cos \sigma + \frac{1}{2(\mu_{2q}^2 + (2\nu_q - \nu_{2q})^2)} (\mu_{2q}(\delta_1\rho_1 + \delta_2\rho_2) \\ & + \mu_{2q}(\delta_1\rho_1 - \delta_2\rho_2) \cos 2\sigma + (2\nu_q - \nu_{2q})(\delta_1\rho_2 - \delta_2\rho_1) \sin 2\sigma). \end{aligned} \quad (4.10)$$

Here by the translation symmetry, Eq. (4.8) must depend only on r and μ , even if the higher-order terms are included. We take such a sufficiently large value for b_3 as $\beta_\sigma > 0$. Noting that $\nu_q > 0$ for $\kappa > 0$ by Proposition 3.3, we easily show that a Hopf bifurcation [26, 29, 35] occurs in (4.8) as follows (cf. Fig. 2):

- (i) The equilibrium $r = 0$ is stable for $\mu > 0$ and unstable for $\mu < 0$;
- (ii) There exists a stable periodic orbit given by

$$r = \sqrt{-\frac{\mu}{\beta_\sigma}} + O(\mu), \quad \psi = \nu_q t + O(\sqrt{\mu}), \quad (4.11)$$

for $\mu < 0$.

From this result, we obtain the following for the CL (1.10).

TABLE 1. Constants appearing in Eq. (4.10) for $\kappa = 0.4, 0.5$. The numbers are rounded up to the fifth decimal point.

κ	0.4				0.5
q	1	2	3	4	[4]
$\frac{b_{1q}}{\cos \sigma}$	0.13722	0.52798	0.31468	0.46570	0.5
β_1	0.07400	0.25258	0.16495	0.23150	0.25
δ_1	-0.45414	-0.46902	-0.35398	-0.38647	-0.5
δ_2	-0.02155	0.04564	-0.03042	0.00539	0
ρ_1	-0.22707	-0.23451	-0.17699	-0.19323	-0.25
ρ_2	-0.12616	-0.20333	-0.19778	-0.21846	-0.25
$\frac{\mu_{2q} + b_{1q}}{\cos \sigma}$	-0.04309	0.09127	-0.06085	0.01077	0
$\frac{\nu_q}{\sin \sigma}$	0.47568	0.423387	0.38441	0.38108	0.5
$\frac{\nu_{2q}}{\sin \sigma}$	0.04309	-0.09127	0.06085	-0.01077	0

Theorem 4.4. *Let $q \in [4]$ and suppose that $\beta_\sigma > 0$, i.e., $b_3 > -\frac{4}{3}\bar{\beta}_{1\sigma}$, and $\mu_j = -b_{1q} + \chi_1(j, q) \cos \sigma < 0$ for any $j \neq q$. Then the following bifurcation of the twisted solution (1.11) occurs at $b_1 = b_{1q}$ in the CL (1.10) with $\sigma \neq 0$:*

- (i) *The twisted solution (1.11) is stable for $b_1 > b_{1q}$ and unstable for $b_1 < b_{1q}$;*
- (ii) *There exists a stable one-parameter family of oscillating twisted solutions*

$$\tilde{\mathcal{U}}^q = \left\{ u = 2\pi qx + \sqrt{-\frac{b_1 - b_{1q}}{\beta_\sigma}} \sin(2\pi qx + \tilde{\psi}(t) + \psi) + \Omega t + O(b_1 - b_{1q}) \mid \psi \in \mathbb{S}^1 \right\} \quad (4.12)$$

for $b_1 < b_{1q}$ near $b_1 = b_{1q}$, where $\tilde{\psi}(t) \in \mathbb{S}^1$ is a periodic function whose period is approximately $2\pi/\nu_q$. Here Ω and $\beta_\sigma = O(1)$ are given in (1.12) and (4.9), respectively.

Remark 4.5.

- (i) *A bifurcation similar to one detected in Theorem 4.4 also occurs at $b_1 = b_{1q}$ even if $b_3 < -\frac{4}{3}\bar{\beta}_{1\sigma}$ or $\mu_j > 0$ although the one-parameter family $\tilde{\mathcal{U}}^q$ of oscillating twisted solutions born there is unstable (cf. Remark 4.3(i)).*
- (ii) *We suspect for any $q \in \mathbb{N}$ that the statements of Theorem 4.4 also hold (cf. Remark 4.3(ii)).*
- (iii) *As in Remark 4.3(iii), the twisted solution (1.11) (resp. $\tilde{\mathcal{U}}^q$) behaves as if it is an asymptotically stable or unstable solution (resp. a asymptotically stable families of solutions) in the KM (1.1) near $b_1 = b_{1q}$ for $n > 0$ sufficiently large. Thus, the KM (1.1) suffers a “bifurcation” similar to one detected in Theorem 4.4 for the CL (1.10).*

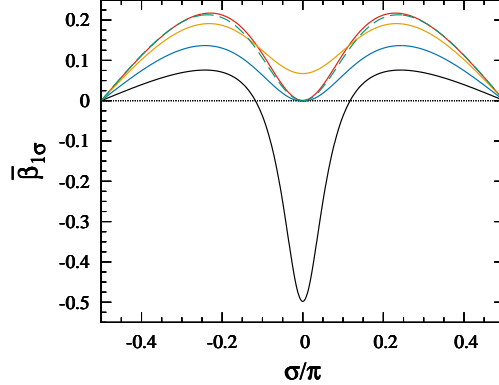


FIGURE 4. Dependence of $\bar{\beta}_{1\sigma}$ on σ for $\kappa = 0.4, 0.5$: The black, red, blue and orange lines represent the cases of $q = 1, 2, 3$ and 4 , respectively, for $\kappa = 0.4$, while the green dashed line represents the case of $q \in [4]$ for $\kappa = 0.5$. Note that $\bar{\beta}_{1\sigma}$ is independent of q when $\kappa = 0.5$.

The values of constants appearing in (4.10) are provided in Table 1 for $q \in [4]$ and $\kappa = 0.4, 0.5$. In particular, when $\kappa = \frac{1}{2}$,

$$\bar{\beta}_{1\sigma} = \frac{3 \cos \sigma \sin^2 \sigma}{2(4 - 3 \cos^2 \sigma)}.$$

Figure 4 shows the dependence of $\beta_{1\sigma}$ on σ for $q \in [4]$ and $\kappa = 0.4, 0.5$. Note that Theorem 4.4 requires $b_3 > -\frac{4}{3}\bar{\beta}_{1\sigma}$ as its hypotheses. In particular, the one-parameter family \mathcal{U}^q born at the bifurcation is stable for $\sigma \neq 0, \pm\frac{1}{2}\pi$ if $q = 2-4$ or $\kappa = 0.5$, and in some range of σ if $q = 1$ and $\kappa = 0.4$, even when $b_3 = 0$.

5. NUMERICAL SIMULATIONS: NEAREST NEIGHBOR GRAPHS

In this and the next sections, we give numerical simulation results for the KM (1.1) with the phase-lag $\sigma = 0$ or $\pi/3$ defined on deterministic $\lfloor n\kappa \rfloor$ -nearest neighbor and complete simple graphs, respectively. Here we assume

$$\omega = -\frac{\sin(2\pi q\kappa) \sin \sigma}{\pi q} \quad (5.1)$$

without loss of generality, considering an adequate rotational frame if necessary. Note that $\omega = 0$ for $\sigma = 0$ or $\kappa = \frac{1}{2}$ and that the q -twisted solution (1.11) in the CL (1.10) has $\Omega = 0$ by (1.12) for any $\sigma \in (-\frac{1}{2}\pi, \frac{1}{2}\pi)$.

We carried out numerical simulations for the KM (1.1), using the DOP853 solver [28], for $q \in [4]$. We took $n = 1000$ and chose the initial values $u_k^n(0)$, $k \in [n]$, independently randomly according to the uniform distribution on the intervals $[-\pi + 2\pi qk/n, \pi + 2\pi qk/n]$ centered at the q -twisted state (1.6) with $\Omega_D = 0$. So if there is an asymptotically stable that are different from the twisted and modulated or oscillating twisted states, then the responses of (1.1) may converge to it as $t \rightarrow \infty$. We also considered two cases $\sigma = 0$ and $\pi/3$ for the phase lag, and $\kappa = 0.4$ and 0.5 for the neighbor size. Recall that the κ -nearest neighbor graph reduce to a complete simple one when $\kappa = 0.5$.

We begin with numerical results for κ -nearest neighbor graphs with $\kappa = 0.4$, for which the q -twisted solution (1.11) is unstable in the uncontrolled CL (1.10) with $b_1, b_3 = 0$, since condition (3.1) does not hold for $\ell = q \in [4]$ when $b_1 = 0$ as seen from Table 1. The results for $\kappa = 0.5$ are provided in the next section.

Figures 5 and 6 show the time-histories of every 100th node (from 50th to 950th) for $\sigma = 0$ and $\pi/3$, respectively. The values of b_1 in the left and right columns of each figure were chosen such that they are larger and smaller, respectively, than the bifurcation points, which are approximated by b_{1q} , $q \in [4]$, (see Eq. (4.1)) for the q -twisted solutions (1.11) in the CL (1.10). We see that the responses of the KM (1.1) converge to their steady states rapidly although their initial values are randomly distributed on the wide interval. Moreover, oscillations occur for the smaller values of b_1 when $\sigma = \pi/3$, in the right column of Fig. 6, as detected by Theorem 4.4 for the CL (1.10). We also notice that no rotation is observed even when $\sigma = \pi/3$, like the q -twisted solution (1.11) in the CL (1.10), in contrast to observations for the uncontrolled KM (1.1) with $b_1, b_3 = 0$ in [70].

In Figs. 7 and 8, $u_k^n(t)$, $k \in [n]$, at $t = 1000$, which may be regarded as the steady states from Figs. 5 and 6, are plotted as small red disks for $\sigma = 0$ and $\pi/3$, respectively. Here the same values of b_1 and $u_k^n(0)$, $k \in [n]$, as in Figs. 5 and 6 were used. We observe that the responses of the KM (1.1) converge to the twisted and modulated or oscillating twisted states, respectively, for the larger and smaller values of b_1 , as predicted by Theorems 4.2 and 4.4 with the assistance of Corollary 2.5 and Theorem 2.8. Indeed, we confirmed that the deviation from the twisted state is about 10^{-7} at most in the left column of each figure for the larger values of b_1 . In particular, the target state (1.6) is accomplished there.

The most probably leading term,

$$u(x) = 2\pi qx + r(t) \sin(2\pi qx + \psi(t)) + \Omega t, \quad (5.2)$$

in the modulated and oscillating twisted solutions (4.7) and (4.12) was estimated from the numerical simulation results for each cases by using the least mean square method as

$$\Omega t = \frac{1}{n} \sum_{k=1}^n v_k^n(t), \quad r(t) = 2\sqrt{c(t)^2 + s(t)^2} \quad (5.3)$$

and

$$\psi(t) = \arctan \frac{s(t)}{c(t)} \quad \left(\text{resp. } \arctan \frac{s(t)}{c(t)} + pi \text{ or } \arctan \frac{s(t)}{c(t)} - \pi \right)$$

for $c(t) > 0$ (resp. $c(t) < 0$ and $s(t) > 0$ or $s(t) < 0$) with

$$v_k^n(t) = u_k^n(t) - \frac{2\pi qk}{n}$$

and

$$c(t) = \frac{1}{n} \sum_{k=1}^n v_k^n(t) \cos \frac{2\pi k}{n}, \quad s(t) = \frac{1}{n} \sum_{k=1}^n v_k^n(t) \sin \frac{2\pi k}{n},$$

and it is plotted as a blue line in each figure. The computed results coincide with the simulation results for the KM (1.1) almost completely, as detected by Theorems 4.2 and 4.4 for the CL (1.10). Here the estimated values of Ωt in (5.3) were very small, and more precisely about 10^{-12} and 10^{-2} at most for $\sigma = 0$ and $\pi/3$, respectively, even when $t = 1000$.

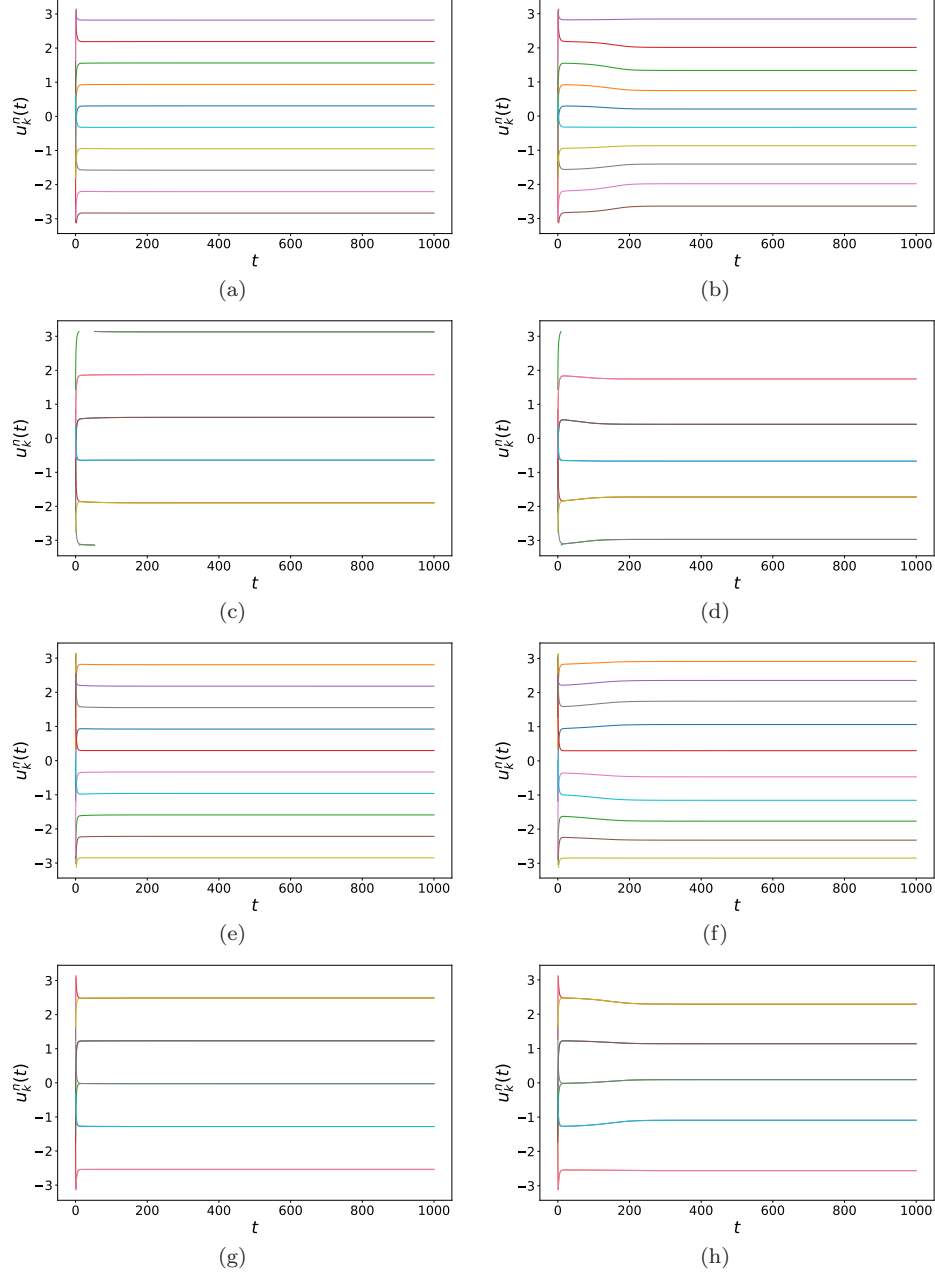


FIGURE 5. Numerical simulation results for the KM (1.1) with $n = 1000$, $\kappa = 0.4$ and $\sigma = 0$: (a) $(q, b_1, b_3) = (1, 0.16, 1)$; (b) $(1, 0.12, 1)$; (c) $(2, 0.55, 0.5)$; (d) $(2, 0.51, 0.5)$; (e) $(3, 0.34, 0.5)$; (f) $(3, 0.3, 0.5)$; (g) $(4, 0.49, 0.5)$; (h) $(4, 0.45, 0.5)$. The values of $u_k^n(t) \bmod 2\pi$, $k \in [n]$, are plotted as the ordinates. The five pairs of two lines coincide almost completely in Figs. (c), (d), (g) and (h).

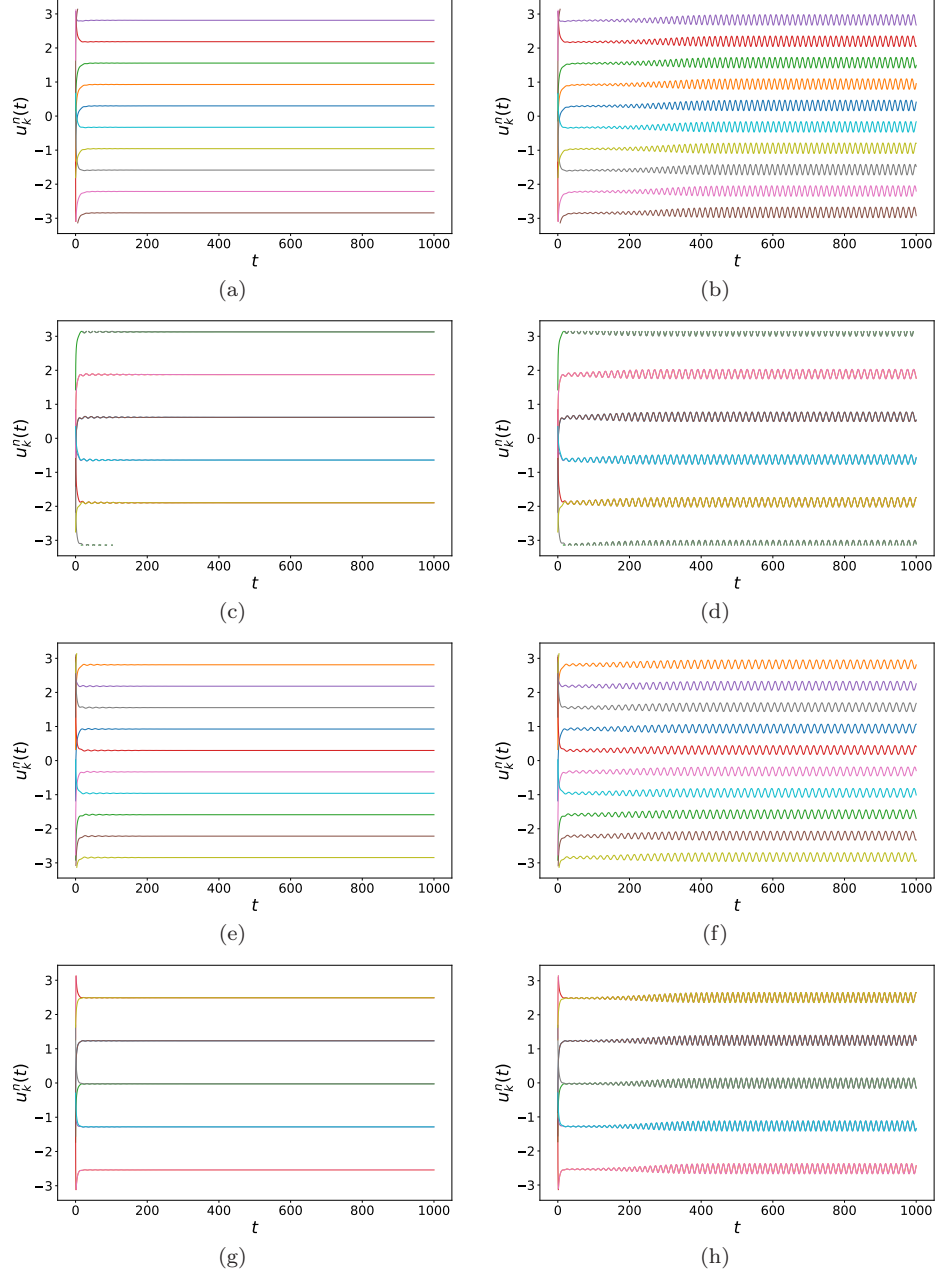


FIGURE 6. Numerical simulation results for the KM (1.1) with $n = 1000$, $\kappa = 0.4$, $\sigma = \pi/3$ and $b_3 = 0.5$: (a) $(q, b_1) = (1, 0.08)$; (b) $(1, 0.06)$; (c) $(2, 0.275)$; (d) $(2, 0.255)$; (e) $(3, 0.17)$; (f) $(3, 0.15)$; (g) $(4, 0.245)$; (h) $(4, 0.225)$. See also the caption of Fig. 5.

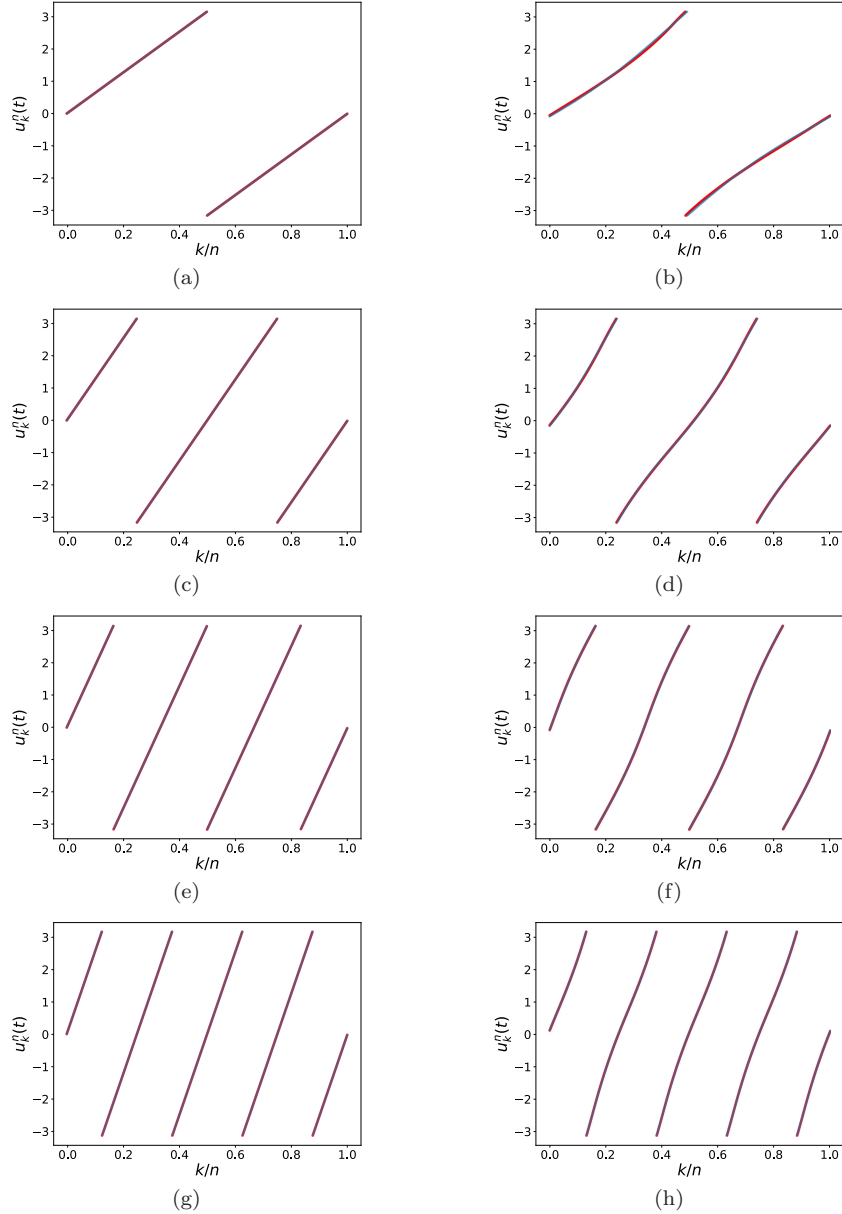


FIGURE 7. Steady states of the KM (1.1) with $n = 1000$ and $\sigma = 0$ at $t = 1000$: (a) $(q, b_1, b_3) = (1, 0.16, 1)$; (b) $(1, 0.12, 1)$; (c) $(2, 0.55, 0.5)$; (d) $(2, 0.51, 0.5)$; (e) $(3, 0.34, 0.5)$; (f) $(3, 0.3, 0.5)$; (g) $(4, 0.49, 0.5)$; (h) $(4, 0.45, 0.5)$. The values of $u_k^n(t) \bmod 2\pi$, $k \in [n]$, are plotted as the ordinates. The simulation results are plotted as small red disks and the most probable leading terms in (4.7) and (4.12) estimated from them as blue lines although they coincide almost completely.

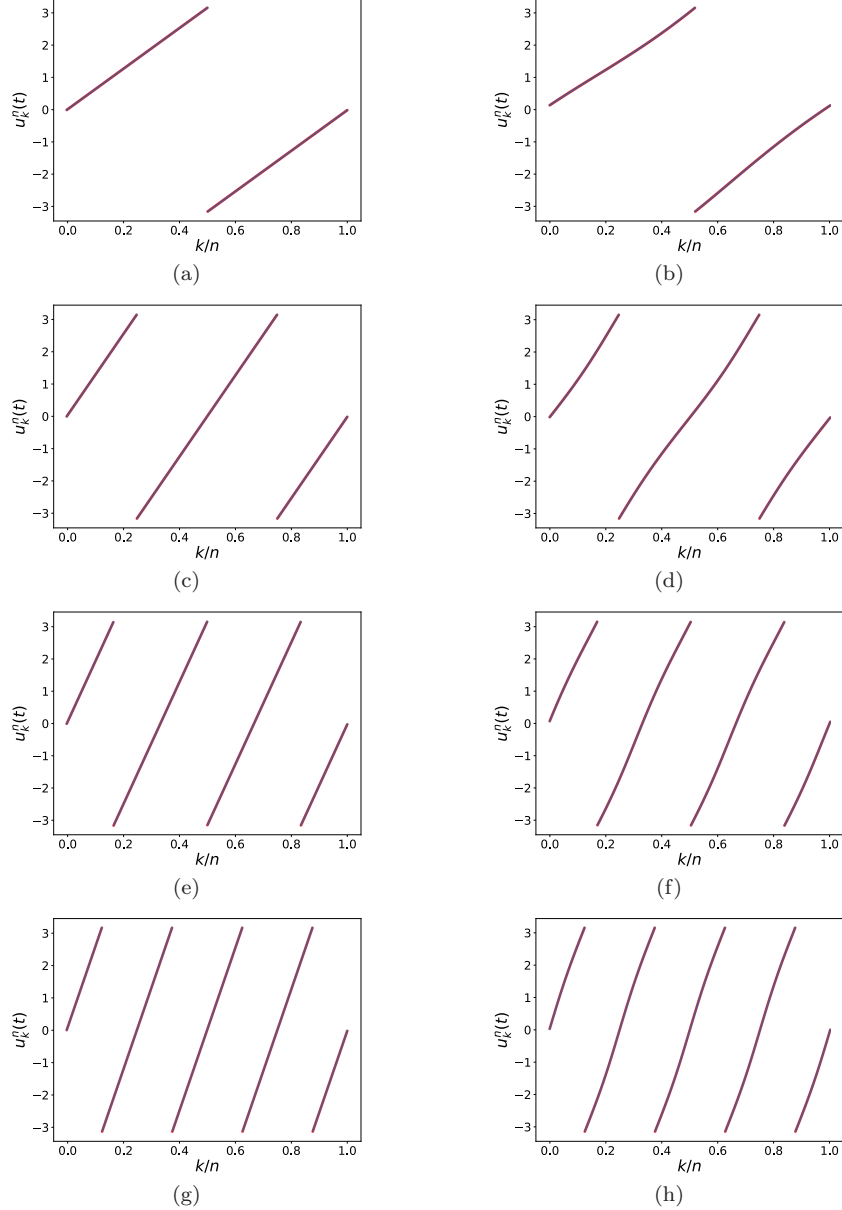


FIGURE 8. Steady states of the KM (1.1) with $n = 1000$, $\sigma = \pi/3$ and $b_3 = 0.5$ at $t = 1000$: (a) $(q, b_1) = (1, 0.08)$; (b) $(1, 0.06)$; (c) $(2, 0.275)$; (d) $(2, 0.255)$; (e) $(3, 0.17)$; (f) $(3, 0.15)$; (g) $(4, 0.245)$; (h) $(4, 0.225)$. See also the caption of Fig. 7.

In Figs. 9 and 10, the deviation, $u_k^n(t) - 2\pi qk/n$, $k \in [n]$, of the steady state in the right columns of Figs. 7 and 8 from the q -twisted state (1.6) in the KM (1.1) for $\sigma = 0$ and $\sigma = \pi/3$, respectively, when b_1 is considered to be smaller than the bifurcation point, is plotted as small red disks. It was also estimated from the most

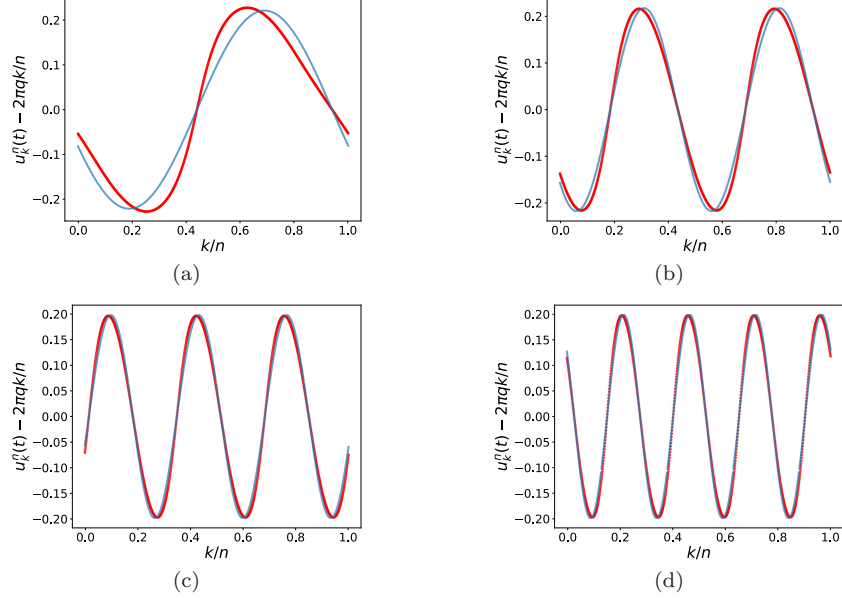


FIGURE 9. Deviation from the q -twisted states in the steady states of the KM (1.1) with $n = 1000$ and $\sigma = 0$ at $t = 1000$: (a) $(q, b_1, b_3) = (1, 0.12, 1)$; (b) $(2, 0.51, 0.5)$; (c) $(3, 0.3, 0.5)$; (d) $(4, 0.45, 0.5)$. The simulation results are plotted as small red disks, and the estimates from their most probably leading terms given by (5.2) are plotted as blue lines.

probably leading term displayed in Figs. 7 and 8 and is plotted as a blue line. The agreement between both results is fine except in Fig. 9(a) for $q = 1$ and $\kappa = 0.4$. The reason for their disagreement in Fig. 9(a) is considered to be that the absolute value of $\mu_{2q} = (\chi_1(2q, q) - \chi_1(q, q)) \cos \sigma$ is small and the $2q$ -oscillation mode is easily to be excited when $q = 1$ and $\kappa = 0.4$ (see Fig. 1), compared with the other cases.

Finally, we present numerically computed bifurcation diagrams for $\sigma = 0$ and $\pi/3$ in Figs. 11 and 12, respectively. The amplitude r of the expression (5.2) estimated from the numerical simulation results for the steady states as in Figs. 7-10 are plotted as small red disks, and the theoretical predictions,

$$\sqrt{-\frac{b_1 - b_{1q}}{\beta_0}} \quad \text{and} \quad \sqrt{-\frac{b_1 - b_{1q}}{\beta_\sigma}}, \quad (5.4)$$

obtained from Theorems 4.2 and 4.4 are plotted as black solid lines for $\sigma = 0$ and $\sigma = \pi/3$, respectively, where β_0 and β_σ are given by (4.6) and (4.9). Good agreement between both results is found, especially in Figs. 11(b) and (c), although slight differences are seen in the other figures.

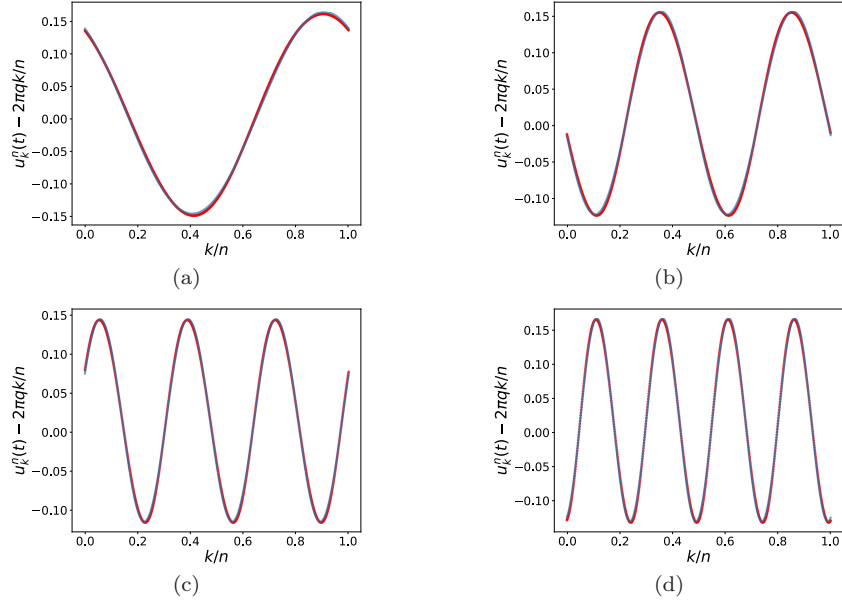


FIGURE 10. Deviation from the q -twisted states in the steady states of the KM (1.1) with $n = 1000$, $\sigma = \pi/3$ and $b_3 = 0.5$ at $t = 1000$: (a) $(q, b_1) = (1, 0.06)$; (b) $(2, 0.255)$; (c) $(3, 0.15)$; (d) $(4, 0.225)$. See also the caption of Fig. 9.

6. NUMERICAL SIMULATIONS: COMPLETE SIMPLE GRAPHS

We next give numerical results for complete simple graphs, i.e., $\kappa = \frac{1}{2}$, for which the q -twisted solutions given by (1.13) still exists but is unstable in the uncontrolled CL (1.10) with $b_1, b_3 = 0$.

Figures 13 and 14 show the time-histories of every 100th node (from 50th to 950th) for $\sigma = 0$ and $\pi/3$, respectively, like Figs. 5 and 6. Here the values of $u_k^n(t) \bmod 2\pi$, $k \in [n]$, are plotted as the ordinates. The values of $b_1 = 0.52$ and 0.48 (resp. $b_1 = 0.26$ and 0.24) were chosen in the left and right columns of Fig. 13 (resp. of Fig. 14), respectively, and they are larger and smaller than the bifurcation point approximated by $b_{1q} = 0.5$ (resp. $b_{1q} = 0.25$) (see Table. 1). We see that the responses converge to the steady states rapidly, and oscillations occur in the right column of Fig. 14 for $\sigma = \pi/3$ and $b_1 = 0.24$, as detected by Theorem 4.4 for the CL (1.10).

In Figs. 15 and 16, $u_k^n(t)$, $k \in [n]$, at $t = 1000$, which may be regarded as the steady states from the results of Figs. 13 and 14, are plotted as small red disks for $\sigma = 0$ and $\pi/3$, respectively. Here the same values of b_1 and $u_k^n(0)$, $k \in [n]$, as in Figs. 13 and 14 were used. We observe that the responses of the KM (1.1) converge to the twisted and modulated or oscillating twisted states for $b_1 = 0.52$ or 0.26 and 0.48 or 0.24 in the left and right columns of each figure, respectively, as predicted by Theorems 4.2 and 4.4 with the assistance of Corollary 2.5 and Theorem 2.8. Indeed, we confirmed that the deviation from the twisted state is about 10^{-11} and 10^{-6} at most in the left columns of Figs. 15 and 16 for $b_1 = 0.52$ and 0.26 , respectively. In particular, the target state (1.6) is accomplished there. The most probably leading

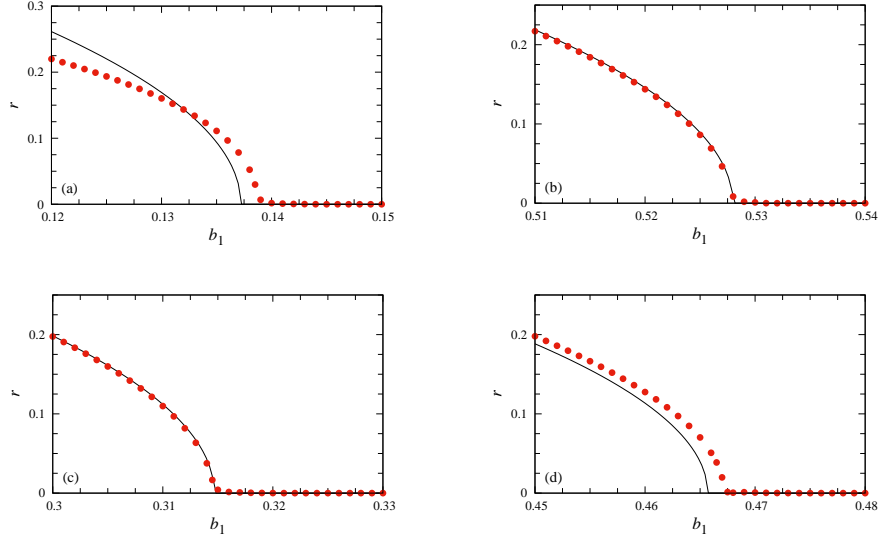


FIGURE 11. Bifurcation diagram of the steady states in the KM (1.1) with $n = 1000$, $\kappa = 0.4$ and $\sigma = 0$: (a) $(q, b_3) = (1, 1)$; (b) $(2, 0.5)$; (c) $(3, 0.5)$; (d) $(4, 0.5)$. The amplitude r in (5.2) estimated from the simulation results and theoretical predictions (see the text for more details) are plotted as small red disks and black solid lines, respectively.

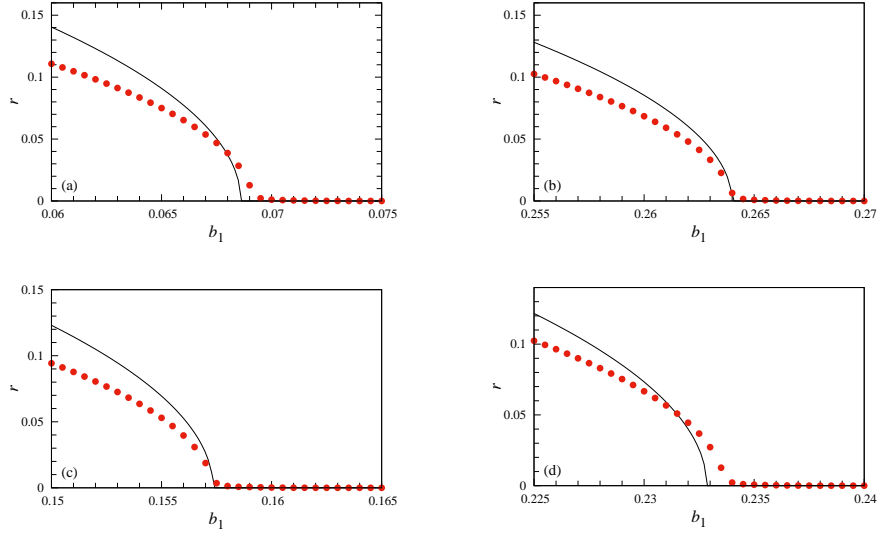


FIGURE 12. Bifurcation diagram of the steady states in the KM (1.1) with $n = 1000$, $\kappa = 0.4$, $\sigma = \pi/3$ and $b_3 = 0.5$: (a) $q = 1$; (b) 2; (c) 3; (d) 4. See also the caption of Fig. 11.

term (5.2) in the modulated and oscillating twisted solutions (4.7) and (4.12) was also estimated from the numerical simulation results by using the least mean square

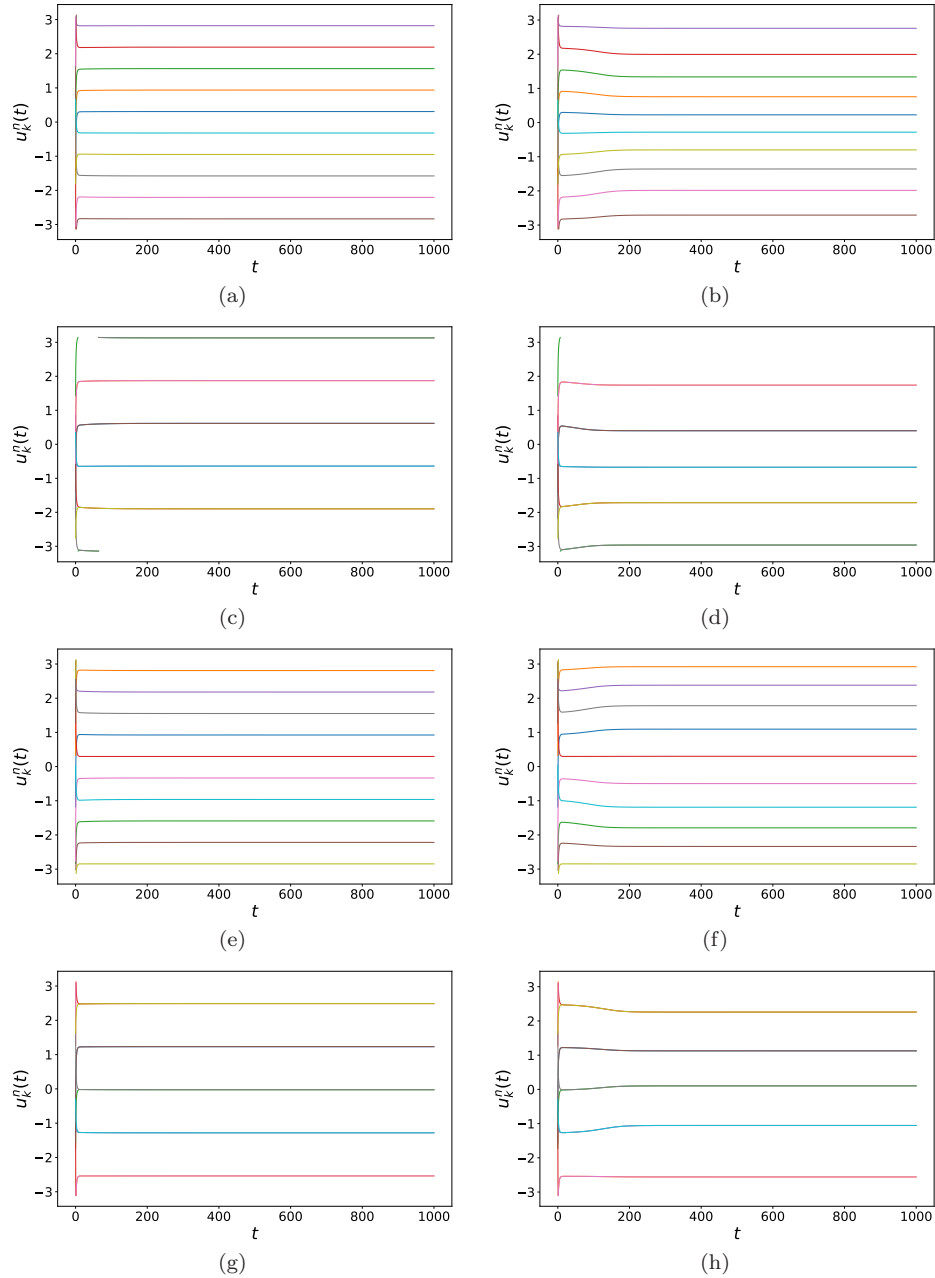


FIGURE 13. Numerical simulation results for the KM (1.1) with $n = 1000$, $\kappa = 0.5$, $\sigma = 0$ and $b_3 = 0.5$: (a) $(q, b_1) = (1, 0.52)$; (b) $(1, 0.48)$; (c) $(2, 0.52)$; (d) $(2, 0.48)$; (e) $(3, 0.52)$; (f) $(3, 0.48)$; (g) $(4, 0.52)$; (h) $(4, 0.48)$. See also the caption of Fig. 5.

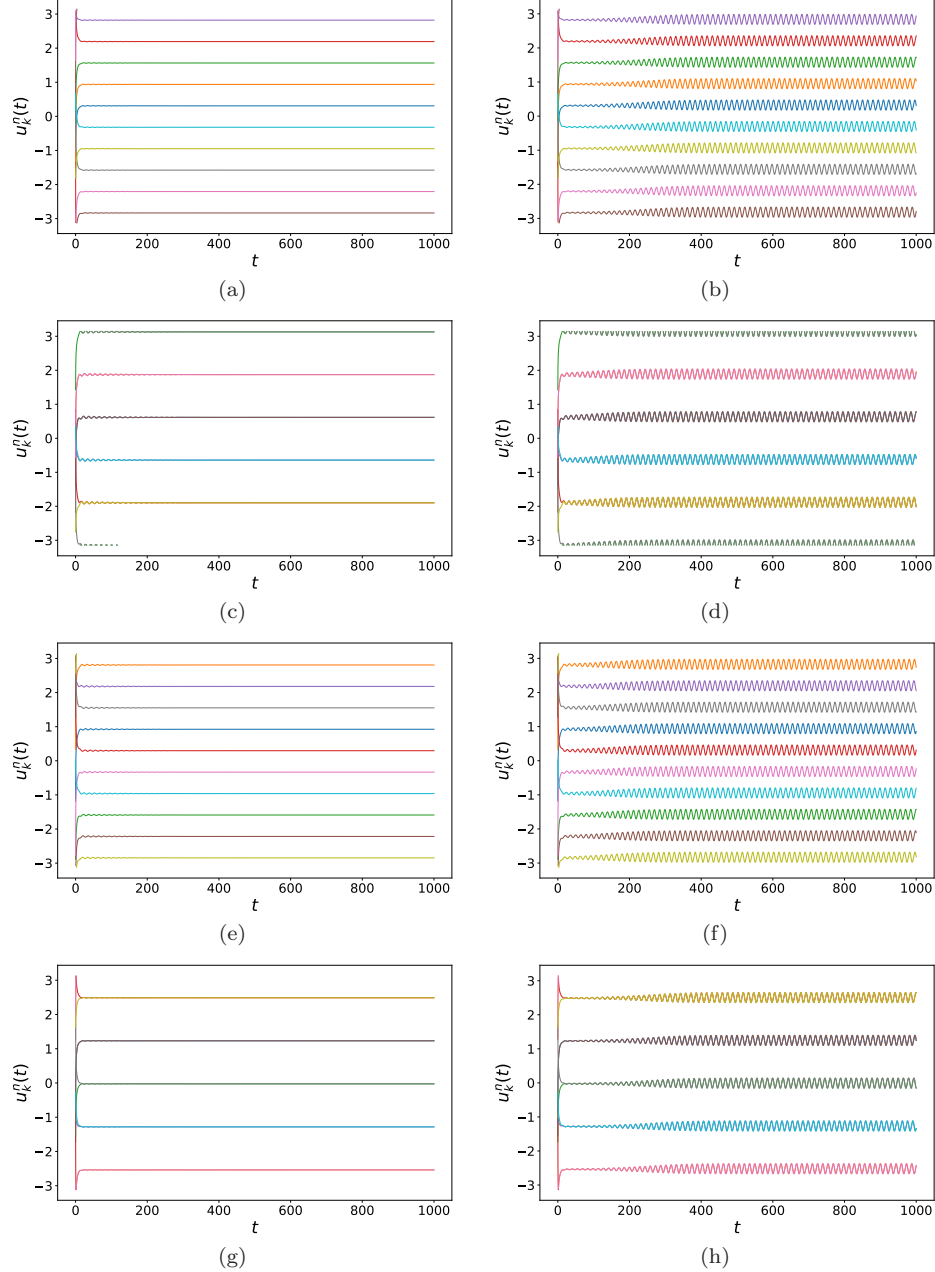


FIGURE 14. Numerical simulation results for the KM (1.1) with $n = 1000$, $\kappa = 0.5$, $\sigma = \pi/3$ and $b_3 = 0.5$: (a) $(q, b_1) = (1, 0.26)$; (b) $(1, 0.24)$; (c) $(2, 0.26)$; (d) $(2, 0.24)$; (e) $(3, 0.26)$; (f) $(3, 0.24)$; (g) $(4, 0.26)$; (h) $(4, 0.24)$. See also the caption of Fig. 5.

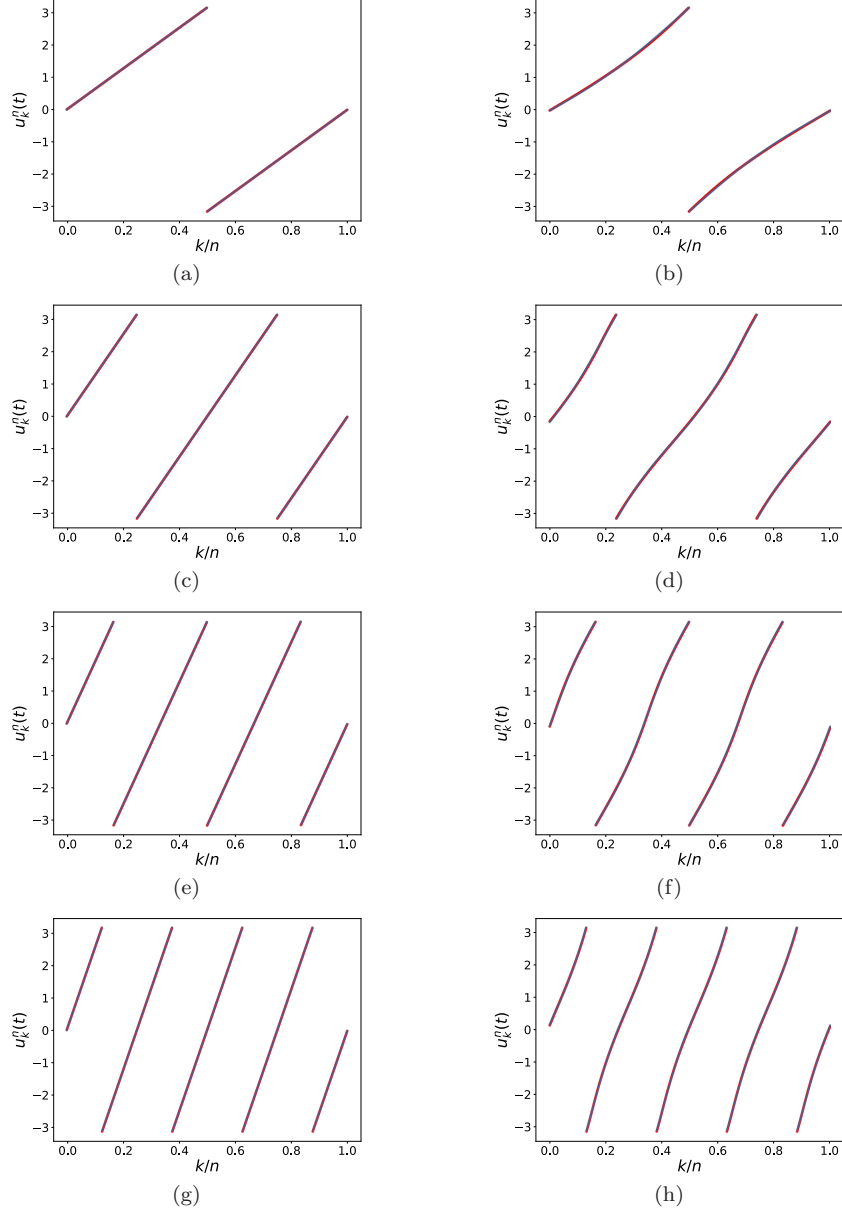


FIGURE 15. Steady states of the KM (1.1) with $n = 1000$, $\kappa = 0.5$, $\sigma = 0$ and $b_3 = 0.5$ at $t = 1000$: (a) $(q, b_1) = (1, 0.52)$; (b) $(1, 0.48)$; (c) $(2, 0.52)$; (d) $(2, 0.48)$; (e) $(3, 0.52)$; (f) $(3, 0.48)$; (g) $(4, 0.52)$; (h) $(4, 0.48)$. See also the caption of Fig. 7.

method and is plotted as a blue line in each figure, as in Figs. 7 and 8. Both results coincide almost completely, as detected by Theorems 4.2 and 4.4 for the CL (1.10).

In Figs. 17 and 18, the deviation, $u_k^n(t) - 2\pi qk/n$, $k \in [n]$, of the steady state in the right columns of Figs. 15 and 16 from the desired q -twisted one in the KM

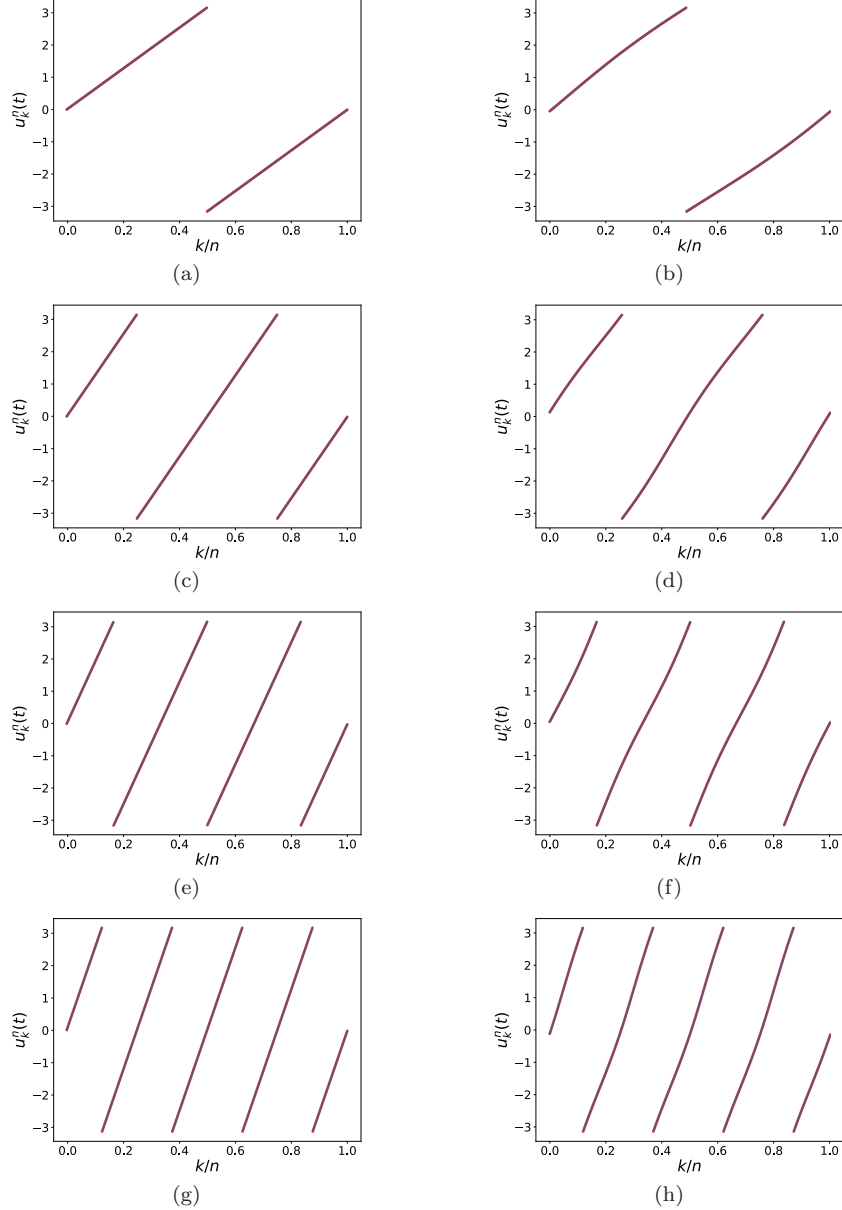


FIGURE 16. Steady states of the KM (1.1) with $n = 1000$, $\kappa = 0.5$, $\sigma = \pi/3$ and $b_3 = 0.5$ at $t = 1000$: (a) $(q, b_1) = (1, 0.26)$; (b) $(1, 0.24)$; (c) $(2, 0.26)$; (d) $(2, 0.24)$; (e) $(3, 0.26)$; (f) $(3, 0.24)$; (g) $(4, 0.26)$; (h) $(4, 0.24)$. See also the caption of Fig. 7.

(1.1) with $\sigma = 0$ and $\sigma = \pi/3$, respectively, is plotted as small red disks. Estimates obtained from the most probably leading terms displayed in Figs. 15 and 16 are also plotted as blue lines, as in Figs. 9 and 10. Both results coincide almost completely.

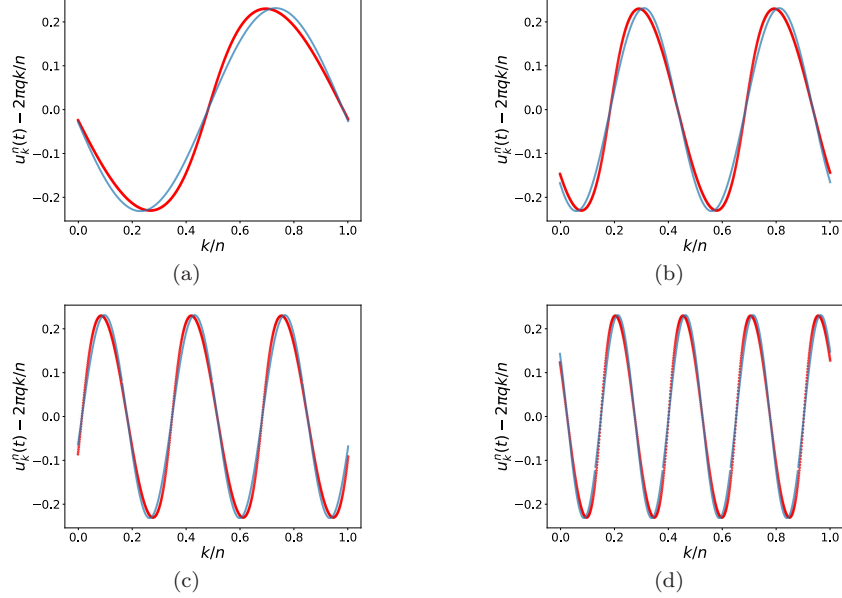


FIGURE 17. Deviation from the q -twisted states in the steady states in the KM (1.1) with $n = 1000$, $\kappa = 0.5$, $\sigma = 0$ and $b_1 = 0.48$ and $b_3 = 0.5$: (a) $q = 1$; (b) 2; (c) 3; (d) 4. See also the caption of Fig. 9.

Finally, we present numerically computed bifurcation diagrams for $\sigma = 0$ and $\pi/3$ in Figs. 19 and 20, respectively, as in Figs. 11 and 12. The amplitude r of (5.2) estimated from the numerical simulation results are plotted as small red disks, and the theoretical predictions given by (5.4) are plotted as black solid lines. Good agreement between both results is found, especially in Fig. 19, although slight differences are seen in Fig. 20.

7. CONCLUDING REMARKS

We summarize this paper as follows: We studied feedback control of twisted states in the KM (1.1) of identical oscillators defined on deterministic nearest neighbor graphs containing complete simple ones when it may have phase-lag. Using the center manifold reduction technique [29], we analyzed the stability and bifurcations of twisted solutions in the CL (1.10) for the KM (1.1) subjected to feedback control. In particular, it was shown that the twisted solutions exist and can be stabilized not only for nearest neighbor graphs but also for complete simple graphs. Moreover, the CL (1.10) was shown to suffer bifurcations at which the twisted solutions becomes unstable and a stable one-parameter family of modulated or oscillating twisted solutions is born, depending on whether the phase-lag is zero or not. We demonstrated the theoretical results by numerical simulations for the feedback controlled KM (1.1) on deterministic nearest neighbor and complete simple graphs.

Finally, we give some comments for future work. The KM and its generalization with phase-lag was studied for different solutions from twisted ones in [5, 11, 37, 44, 47, 50, 51]. In particular, chimera states were discussed in [5, 44, 50]. The theory

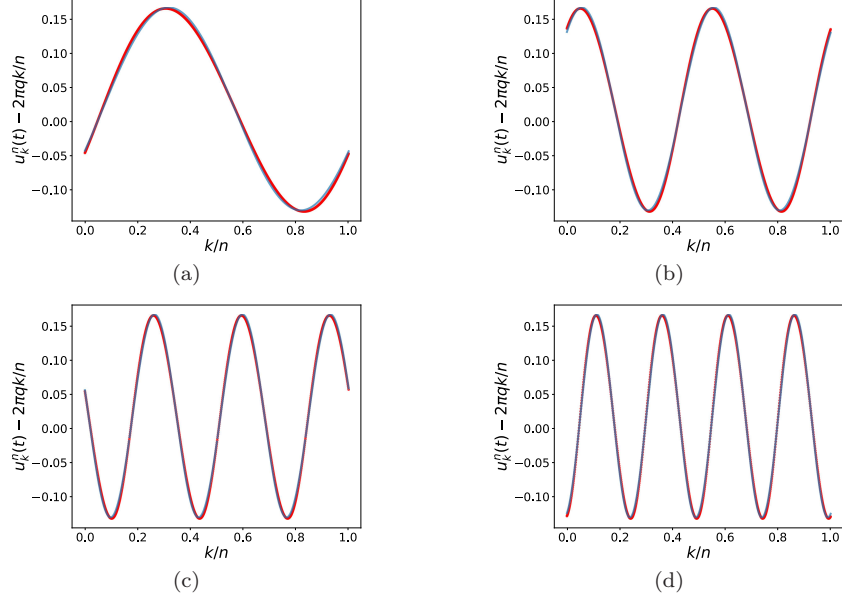


FIGURE 18. Deviation from the q -twisted states in the steady states in the KM (1.1) with $n = 1000$, $\kappa = 0.5$, $\sigma = \pi/3$, $b_1 = 0.24$ and $b_3 = 0.5$: (a) $q = 1$; (b) 2; (c) 3; (d) 4. See also the caption of Fig. 9.

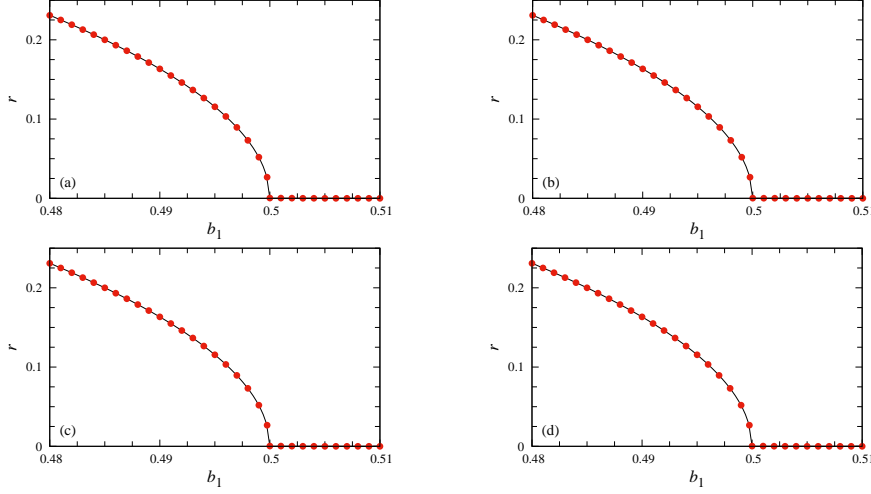


FIGURE 19. Bifurcation diagram of the steady states in the KM (1.1) with $n = 1000$, $\kappa = 0.5$, $\sigma = 0$ and $b_3 = 0.5$: (a) $q = 1$; (b) 2; (c) 3; (d) 4. See also the caption of Fig. 11.

reviewed in Section 2 is also applicable to these cases and may be useful to uncover their dynamics. The KM with time delay, which possesses important applications in neuroscience [9, 14, 20], has often been a subject of research [1, 4, 47, 52, 55]. It

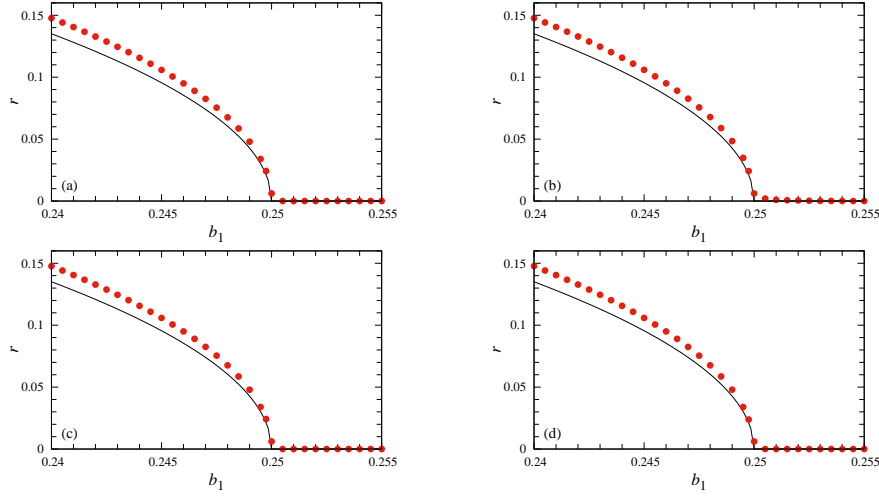


FIGURE 20. Bifurcation diagram of the steady states in the KM (1.1) with $n = 1000$, $\kappa = 0.5$, $\sigma = \pi/3$ and $b_3 = 0.5$: (a) $q = 1$; (b) 2; (c) 3; (d) 4. See also the caption of Fig. 11.

will be another next target to extend the theory of Section 2 to the KM with time delay and its CL.

ACKNOWLEDGEMENTS

This work was partially supported by the JSPS KAKENHI Grant Number JP23K22409. The author thanks the anonymous referees for their helpful comments and constructive suggestions. In particular, by one of them, he could realize an error in Theorem 2.3 of the original manuscript and correct it.

APPENDIX A. DERIVATION OF (4.3)

We first rewrite the CL (1.10) in the rotational frame with the rotational speed Ω as

$$\begin{aligned}
 \frac{\partial}{\partial t}u(t, x) = & \omega - \Omega + p \left(\cos u(t, x) \int_{x-\kappa}^{x+\kappa} \sin u(t, y) dy \right. \\
 & \left. - \sin u(t, x) \int_{x-\kappa}^{x+\kappa} \cos u(t, y) dy \right) \cos \sigma \\
 & + p \left(\sin u(t, x) \int_{x-\kappa}^{x+\kappa} \sin u(t, y) dy \right. \\
 & \left. + \cos u(t, x) \int_{x-\kappa}^{x+\kappa} \cos u(t, y) dy \right) \sin \sigma \\
 & - b_1(\bar{u}(t, x) - u(t, x)) - b_3(\bar{u}(t, x) - u(t, x))^3. \tag{A.1}
 \end{aligned}$$

Letting (4.2) with $\Omega = 0$, we have

$$\begin{aligned} \cos u(t, x) = & \cos 2\pi qx - \sin 2\pi qx \left(\xi_0 + \sum_{j=1}^{\infty} (\xi_j \cos 2\pi jx + \eta_j \sin 2\pi jx) \right) \\ & - \cos 2\pi qx \left(\frac{1}{4}((\xi_q^2 + \eta_q^2) + (\xi_q^2 - \eta_q^2) \cos 4\pi qx + 2\xi_q \eta_q \sin 4\pi qx) \right. \\ & \quad \left. + \xi_0 (\xi_q \cos 2\pi qx + \eta_q \sin 2\pi qx) \right. \\ & \quad \left. + \frac{1}{2} \sum_{j \neq q} ((\xi_q \xi_j + \eta_q \eta_j) \cos 2\pi(q-j)x - (\xi_q \eta_j - \xi_j \eta_q) \sin 2\pi(q-j)x) \right. \\ & \quad \left. + (\xi_q \xi_j - \eta_q \eta_j) \cos 2\pi(q+j)x + (\xi_q \eta_j + \xi_j \eta_q) \sin 2\pi(q+j)x) \right) \\ & + \sin 2\pi qx \left(\frac{1}{8}(\xi_q^2 + \eta_q^2)(\xi_q \cos 2\pi qx + \eta_q \sin 2\pi qx) \right. \\ & \quad \left. + \frac{1}{24}((\xi_q^2 - 3\eta_q^2)\xi_q \cos 6\pi qx + (3\xi_q^2 - \eta_q^2)\eta_q \sin 6\pi qx) \right) + \dots \end{aligned}$$

and

$$\begin{aligned} \sin u(t, x) = & \sin 2\pi qx + \cos 2\pi qx \left(\xi_0 + \sum_{j=1}^{\infty} (\xi_j \cos 2\pi jx + \eta_j \sin 2\pi jx) \right) \\ & - \sin 2\pi qx \left(\frac{1}{4}((\xi_q^2 + \eta_q^2) + (\xi_q^2 - \eta_q^2) \cos 4\pi qx + 2\xi_q \eta_q \sin 4\pi qx) \right. \\ & \quad \left. + \xi_0 (\xi_q \cos 2\pi qx + \eta_q \sin 2\pi qx) \right. \\ & \quad \left. + \frac{1}{2} \sum_{j \neq q} ((\xi_q \xi_j + \eta_q \eta_j) \cos 2\pi(q-j)x - (\xi_q \eta_j - \xi_j \eta_q) \sin 2\pi(q-j)x) \right. \\ & \quad \left. + (\xi_q \xi_j - \eta_q \eta_j) \cos 2\pi(q+j)x + (\xi_q \eta_j + \xi_j \eta_q) \sin 2\pi(q+j)x) \right) \\ & - \cos 2\pi qx \left(\frac{1}{8}(\xi_q^2 + \eta_q^2)(\xi_q \cos 2\pi qx + \eta_q \sin 2\pi qx) \right. \\ & \quad \left. + \frac{1}{24}((\xi_q^2 - 3\eta_q^2)\xi_q \cos 6\pi qx + (3\xi_q^2 - \eta_q^2)\eta_q \sin 6\pi qx) \right) + \dots, \end{aligned}$$

where ‘…’ represents higher-order terms of

$$O \left(\xi_q^4 + \eta_q^4 + \xi_0^2 + \sum_{j=1, j \neq q}^{\infty} (\xi_j^2 + \eta_j^2) \right).$$

We compute the integrals in (A.1) as

$$\begin{aligned} & \int_{x-\kappa}^{x+\kappa} \cos u(t, y) dy \\ = & -a_2(q, 0) \cos 2\pi qx + a_2(q, 0) \xi_0 \sin 2\pi qx \\ & - \sum_{j=1}^{\infty} (a_1(q, j) (\xi_j \sin 2\pi jx - \eta_j \cos 2\pi jx) \cos 2\pi qx \\ & \quad - a_2(q, j) (\xi_j \cos 2\pi jx + \eta_j \sin 2\pi jx) \sin 2\pi qx) \\ & + \frac{1}{4} a_2(q, 0) (\xi_q^2 + \eta_q^2) \cos 2\pi qx \\ & + \frac{1}{4} a_1(q, 2q) ((\xi_q^2 - \eta_q^2) \sin 4\pi qx - 2\xi_q \eta_q \cos 4\pi qx) \sin 2\pi qx \\ & + \frac{1}{4} a_2(q, 2q) ((\xi_q^2 - \eta_q^2) \cos 4\pi qx + 2\xi_q \eta_q \sin 4\pi qx) \cos 2\pi qx \\ & + \frac{1}{8} a_1(q, q) (\xi_q^2 + \eta_q^2) (\xi_q \sin 2\pi qx - \eta_q \cos 2\pi qx) \cos 2\pi qx \\ & - \frac{1}{8} a_2(q, q) (\xi_q^2 + \eta_q^2) (\xi_q \cos 2\pi qx + \eta_q \sin 2\pi qx) \sin 2\pi qx \end{aligned}$$

$$\begin{aligned}
& + \frac{1}{24}a_1(q, 3q)((\xi_q^2 - 3\eta_q^2)\xi_q \sin 6\pi qx - (3\xi_q^2 - \eta_q^2)\eta_q \cos 6\pi qx) \cos 2\pi qx \\
& - \frac{1}{24}a_2(q, 3q)((\xi_q^2 - 3\eta_q^2)\xi_q \cos 6\pi qx + (3\xi_q^2 - \eta_q^2)\eta_q \sin 6\pi qx) \sin 2\pi qx \\
& + a_1(q, q)(\xi_0\xi_q \sin 2\pi qx - \xi_0\eta_q \cos 2\pi qx) \sin 2\pi qx \\
& + a_2(q, q)(\xi_0\xi_q \cos 2\pi qx + \xi_0\eta_q \sin 2\pi qx) \cos 2\pi qx \\
& + \frac{1}{2} \sum_{j \neq q} (a_1(q, q-j)((\xi_q\xi_j + \eta_q\eta_j) \sin 2\pi(q-j)x \\
& \quad + (\xi_q\eta_j - \xi_j\eta_q) \cos 2\pi(q-j)x) \sin 2\pi qx \\
& \quad + a_2(q, q-j)((\xi_q\xi_j + \eta_q\eta_j) \cos 2\pi(q-j)x \\
& \quad \quad - (\xi_q\eta_j - \xi_j\eta_q) \sin 2\pi(q-j)x) \cos 2\pi qx \\
& \quad + a_1(q, q+j)((\xi_q\xi_j - \eta_q\eta_j) \sin 2\pi(q+j)x \\
& \quad \quad - (\xi_q\eta_j + \xi_j\eta_q) \cos 2\pi(q+j)x) \sin 2\pi qx \\
& \quad + a_2(q, q+j)((\xi_q\xi_j - \eta_q\eta_j) \cos 2\pi(q+j)x \\
& \quad \quad + (\xi_q\eta_j + \xi_j\eta_q) \sin 2\pi(q+j)x) \cos 2\pi qx) + \dots
\end{aligned}$$

and

$$\begin{aligned}
& \int_{x-\kappa}^{x+\kappa} \sin u(t, y) dy \\
& = -a_2(q, 0) \sin 2\pi qx - a_2(q, 0)\xi_0 \cos 2\pi qx \\
& \quad - \sum_{j=1}^{\infty} (a_1(q, j)(\xi_j \sin 2\pi jx - \eta_j \cos 2\pi jx) \sin 2\pi qx \\
& \quad \quad + a_2(q, j)(\xi_j \cos 2\pi jx + \eta_j \sin 2\pi jx) \cos 2\pi qx) \\
& \quad + \frac{1}{4}a_2(q, 0)(\xi_q^2 + \eta_q^2) \sin 2\pi qx \\
& \quad - \frac{1}{4}a_1(q, 2q)((\xi_q^2 - \eta_q^2) \sin 4\pi qx - 2\xi_q\eta_q \cos 4\pi qx) \cos 2\pi qx \\
& \quad + \frac{1}{4}a_2(q, 2q)((\xi_q^2 - \eta_q^2) \cos 4\pi qx + 2\xi_q\eta_q \sin 4\pi qx) \sin 2\pi qx \\
& \quad + \frac{1}{8}a_1(q, q)(\xi_q^2 + \eta_q^2)(\xi_q \sin 2\pi qx - \eta_q \cos 2\pi qx) \sin 2\pi qx \\
& \quad + \frac{1}{8}a_2(q, q)(\xi_q^2 + \eta_q^2)(\xi_q \cos 2\pi qx + \eta_q \sin 2\pi qx) \cos 2\pi qx \\
& \quad + \frac{1}{24}a_1(q, 3q)((\xi_q^2 - 3\eta_q^2)\xi_q \sin 6\pi qx - (3\xi_q^2 - \eta_q^2)\eta_q \cos 6\pi qx) \sin 2\pi qx \\
& \quad + \frac{1}{24}a_2(q, 3q)((\xi_q^2 - 3\eta_q^2)\xi_q \cos 6\pi qx + (3\xi_q^2 - \eta_q^2)\eta_q \sin 6\pi qx) \cos 2\pi qx \\
& \quad - a_1(q, q)(\xi_0\xi_q \sin 2\pi qx - \xi_0\eta_q \cos 2\pi qx) \cos 2\pi qx \\
& \quad + a_2(q, q)(\xi_0\xi_q \cos 2\pi qx + \xi_0\eta_q \sin 2\pi qx) \sin 2\pi qx \\
& \quad - \frac{1}{2} \sum_{j \neq q} (a_1(q, q-j)((\xi_q\xi_j + \eta_q\eta_j) \sin 2\pi(q-j)x \\
& \quad \quad + (\xi_q\eta_j - \xi_j\eta_q) \cos 2\pi(q-j)x) \cos 2\pi qx \\
& \quad \quad - a_2(q, q-j)((\xi_q\xi_j + \eta_q\eta_j) \cos 2\pi(q-j)x \\
& \quad \quad \quad - (\xi_q\eta_j - \xi_j\eta_q) \sin 2\pi(q-j)x) \sin 2\pi qx \\
& \quad \quad + a_1(q, q+j)((\xi_q\xi_j - \eta_q\eta_j) \sin 2\pi(q+j)x \\
& \quad \quad \quad - (\xi_q\eta_j + \xi_j\eta_q) \cos 2\pi(q+j)x) \cos 2\pi qx
\end{aligned}$$

$$\begin{aligned}
& -a_2(q, q+j)((\xi_q \xi_j - \eta_q \eta_j) \cos 2\pi(q+j)x \\
& + (\xi_q \eta_j + \xi_j \eta_q) \sin 2\pi(q+j)x) \sin 2\pi qx) + \dots
\end{aligned}$$

We substitute (4.2) into (A.1), integrate the resulting equation with respect to x from 0 to 1 after multiplying it with $\cos 2\pi j$ or $\sin 2\pi j$, $j \in \mathbb{N}$. Thus, we obtain (4.3) for $q \in [4]$ after lengthy calculations.

REFERENCES

- [1] J.A. Acebrón, L.L. Bonilla, C.J. Pérez Vicente, F. Ritort and R. Spigler, The Kuramoto model: A simple paradigm for synchronization phenomena, *Rev. Mod. Phys.*, **77** (2005), 137–185.
- [2] S.A. Aghdam and M. Agamy, Virtual oscillator-based methods for grid-forming inverter control: A review, *IET Renew. Power Gener.*, **16** (2022), 835–855.
- [3] A.V. Andreev, A.A. Badarin, V.A. Maximenko and A.E. Hramov, Forecasting macroscopic dynamics in adaptive Kuramoto network using reservoir computing, *Chaos*, **32** (2022), 103126.
- [4] A. Arenas, A. Diaz-Guilera, J. Kurths, Y. Moreno and C. Zhou, Synchronization in complex networks, *Phys. Rep.*, **469** (2008), 93–153.
- [5] C. Bick, M. Goodfellow, C.R. Laing and E.A. Martens, Understanding the dynamics of biological and neural oscillator networks through exact mean-field reductions: A review, *J. Math. Neurosci.*, **10** (2020), 9.
- [6] S. Boccaletti, V. Latora, Y. Moreno, M. Chavez, D.-U. Hwang, Complex networks: Structure and dynamics, *Phys. Rep.*, **660** (2016), 1–94.
- [7] S. Boccaletti, J.A. Almendral, S. Guan, I. Leyva, Z. Liu, I. Sendiña-Nadal, Z. Wang and Y. Zou, Explosive transitions in complex networks' structure and dynamics: Percolation and synchronization, *Phys. Rep.*, **660** (2016), 1–94.
- [8] M. Breakspear, S. Heitmann and A. Daffertshofer, Generative models of cortical oscillations: neurobiological implications of the Kuramoto model, *Front. Hum. Neurosci.*, **4** (2010), 190.
- [9] R.C. Budzinski, T.T. Nguyen, G.B. Benigno, J. Đoàn, J. Mináč, T.J. Sejnowski and L.E. Muller, Analytical prediction of specific spatiotemporal patterns in nonlinear oscillator networks with distance-dependent time delays, *Phys. Rev. Res.*, **5** (2023), 013159.
- [10] L. Carleson, On convergence and growth of partial sums of Fourier series, *Acta Mathematica*, **116** (1966), 135–157.
- [11] H. Chiba, A center manifold reduction of the Kuramoto-Daido model with a phase-Lag, *SIAM J. Appl. Dyn. Syst.*, **16** (2017), 1235–1259.
- [12] E.A. Coddington and N. Levinson, *Theory of Ordinary Differential Equations*, McGraw-Hill, New York, 1955.
- [13] S.P. Cornelius, W.L. Kath and A.E. Motter, Realistic control of network dynamics, *Nat. Commun.*, **4** (2013), 1942.
- [14] S.M. Crook, G.B. Ermentrout, M.C. Vanier and J.M. Bower, The role of axonal delay in the synchronization of networks of coupled cortical oscillators, *J. Comput. Neurosci.*, **4** (1997), 161–172.
- [15] F. Dörfler and F. Bullo, Synchronization and transient stability in power networks and nonuniform Kuramoto oscillators, *SIAM J. Control Optim.*, **50** (2012), 1616–1642.
- [16] F. Dörfler and F. Bullo, Synchronization in complex networks of phase oscillators: A survey, *Automatica*, **50** (2014), 1539–1564.
- [17] C. Duan, T. Nishikawa and A.E. Motter, Prevalence and scalable control of localized networks, *Proc. Natl. Acad. Sci. USA*, **119** (2022), e2122566119.t
- [18] A.A. Emelianova and V.I. Nekorkin, Synchronization and Chaos in Adaptive Kuramoto Networks with Higher-Order Interactions: A review, *Regul. Chaotic Dyn.*, **30** (2025), 57–75.
- [19] G.B. Ermentrout, Synchronization in a pool of mutually coupled oscillators with random frequencies *J. Math. Biol.*, **22** (1985), 1–9.
- [20] G.B. Ermentrout and T.-W. Ko, Delays and weakly coupled neuronal oscillators, *Philos. Trans. Roy. Soc. A*, **367** (2009), 1097–1115.
- [21] G.B. Ermentrout and T.Y. Park and D. Wilson, Recent advances in coupled oscillator theory, *Philos. Trans. Roy. Soc. A*, **377** (2019), 20190092.
- [22] G. Filatrella, A.H. Nielsen and N. F. Pedersen Analysis of a power grid using a Kuramoto-like model, *Eur. Phys. J. B*, **61** (2008), 485–491.

- [23] A. Franci, A. Chaillet, E. Panteley and F. Lamnabhi-Lagarrigue, Desynchronization and inhibition of Kuramoto oscillators by scalar mean-field feedback, *Math. Control Signals Systems*, **24** (2012), 169–217.
- [24] P. François and V. Mochulska, Waves, patterns, bifurcations: A tutorial review on the vertebrate segmentation clock, *Phys. Rep.*, **1080** (2024), 1-104.
- [25] T. Girnyk, M. Hasler and Y. Maistrenko, Multistability of twisted states in non-locally coupled Kuramoto-type models, *Chaos*, **22** (2012), 013114.
- [26] J. Guckenheimer and P. Holmes, *Nonlinear Oscillations, Dynamical Systems, and Bifurcations of Vector Fields*, Springer, New York, 1983.
- [27] Y. Guo, D. Zhang, Z. Li, Q. Wang and D. Yu, Overviews on the applications of the Kuramoto model in modern power system analysis, *Int. J. Electr. Power Energy. Syst.*, **129** (2021), 106804.
- [28] E. Hairer, S.P. Nørsett and G. Wanner, *Solving Ordinary Differential Equations I: Nonstiff Problems*, 2nd ed. Springer, Berlin, 1993.
- [29] M. Haragus and G. Iooss, *Local Bifurcations, Center Manifolds, and Normal Forms in Infinite-Dimensional Dynamical Systems*, Springer, London, 2011.
- [30] R. Ihara and K. Yagasaki, Continuum limits of coupled oscillator networks depending on multiple sparse graphs, *J. Nonlinear Sci.*, **33** (2023), 62; Correction, **35** (2025), 27.
- [31] D. Kalinzhnyi-Verbovetskyi and G.S. Medvedev, The semilinear heat equation on sparse random graphs, *SIAM J. Math. Anal.*, **49** (2017), 1333-1355.
- [32] D. Kim and K. Yagasaki, Feedback control of the Kuramoto model defined on uniform graphs II: Random natural frequencies, submitted for publication.
- [33] Y. Kuramoto, Self-entrainment of a population of coupled non-linear oscillators, in *International Symposium on Mathematical Problems in Theoretical Physics*, H. Araki (ed.), Springer, Berlin, 1975, pp. 420–422.
- [34] Y. Kuramoto, *Chemical Oscillations, Waves, and Turbulence*, Springer, Berlin, 1984.
- [35] Y.A. Kuznetsov, *Elements of Applied Bifurcation Theory*, Springer, New York, 2004.
- [36] B. Li and K.Y.M. Wong, Optimizing synchronization stability of the Kuramoto model in complex networks and power grids, *Phys. Rev. E*, **95** (2017), 012207.
- [37] T. Li, Y. Xie, Z. Ye, J. Zeng, Y. Liu, L. Liu and Y. Jia, Analysis of synchronization transitions in higher-order Kuramoto oscillator system with different orders of phase lags, *Chaos Solitons Fractals*, **199** (2025), 116749.
- [38] Z. Li and X. Zhao, Synchronization in adaptive Kuramoto oscillators for power grids with dynamic voltages, *Nonlinearity*, **33** (2020), 6624.
- [39] L. Lovász, *Large Networks and Graph Limits*, AMS, Providence RI, 2012.
- [40] G.S. Medvedev, The nonlinear heat equation on dense graphs and graph limits, *SIAM J. Math. Anal.*, **46** (2014), 2743–2766.
- [41] G.S. Medvedev, The nonlinear heat equation on W-random graphs, *Arch. Ration. Mech. Anal.*, **212** (2014), 781–803.
- [42] G.S. Medvedev, Small-world networks of Kuramoto oscillators, *Phys. D*, **266** (2014), 13–22.
- [43] G.S. Medvedev, The continuum limit of the Kuramoto model on sparse random graphs, *Comm. Math. Sci.*, **17** (2019), 883–898.
- [44] G.S. Medvedev and M.S. Mizuhara, Chimeras unfolded, *J. Stat. Phys.*, **186** (2022), 46.
- [45] G.S. Medvedev and J.D. Wright, Stability of twisted states in the continuum Kuramoto model, *SIAM J. Appl. Dyn. Syst.*, **16** (2017), 188–203.
- [46] A. Mishra, S. Saha and S.K. Dana, Chimeras in globally coupled oscillators: A review, *Chaos*, **33** (2023), 092101.
- [47] S. Majih, B. Rakshit, A. Sharma, J. Kurths and D. Ghosh, Dynamical robustness of network of oscillators, *Phys. Rep.*, **1082** (2024), 1–46.
- [48] A.E. Motter, Networkcontrology, *Chaos*, **25** (2015), 097621.
- [49] B. Moyal, P. Rajwani, S. Dutta and S. Jalan, Rotating clusters in phase-lagged Kuramoto oscillators with higher-order interactions, *Phys. Rev. E*, **109** (2024), 034211.
- [50] O.E. Omel'chenko, The mathematics behind chimera states, *Nonlinearity*, **31** (2018), R121–R164.
- [51] O.E. Omel'chenko and M. Wolfrum, Is there an impact of small phase lags in the Kuramoto model? *Chaos*, **16** (2006), 094806.
- [52] A. Pikovsky and M. Rosenblum, Dynamics of globally coupled oscillators: Progress and perspectives, *Chaos*, **25** (2015), 097616.

- [53] A. Pikovsky, M. Rosenblum, and J. Kurths, *Synchronization: A Universal Concept in Non-linear Sciences*, Cambridge University Press, Cambridge, 2001.
- [54] P. Pirker-Díaz, A. Díaz-Guilera and J. Soriano, Self-regulation of a network of Kuramoto oscillators, *Chaos Solitons Fractals*, **184** (2024), 114966.
- [55] F.A. Rodrigues, T.K.DM. Peron, P. Ji and J. Kurths, The Kuramoto model in complex networks, *Phys. Rep.*, **610** (2016), 1–98.
- [56] K. Schmietendorf, O. Kamps, M. Wolff, P.G. Lind, P. Maass and J. Peinke, Bridging between load-flow and Kuramoto-like power grid models: A flexible approach to integrating electrical storage units *Chaos*, **29** (2019), 103151.
- [57] E. Schöll, Synchronization patterns and chimera states in complex networks: Interplay of topology and dynamics, *Eur. Phys. J. Spec. Top.*, **225** (2016), 891–919.
- [58] P. S. Skardal and A. Arenas, Control of coupled oscillator networks with application to microgrid technologies, *Science Advances*, **1** (2015), e1500339.
- [59] P. S. Skardal and A. Arenas, On controlling networks of limit-cycle oscillators, *Chaos*, **26** (2016), 094812.
- [60] J.U. Song, K. Choi, S.M. Oh and B. Kahng, Exploring nonlinear dynamics and network structures in Kuramoto systems using machine learning approaches, *Chaos*, **33** (2023), 073148.
- [61] P. Srivastava, E. Nozari, J.Z. Kim, H. Ju, D. Zhou, C. Becker, F. Pasqualetti, G.J. Pappas, D.S. Bassett, Models of communication and control for brain networks: distinctions, convergence, and future outlook, *Netw. Neurosci.*, **4** (2020), 1122–1159.
- [62] S.H. Strogatz, From Kuramoto to Crawford: Exploring the onset of synchronization in populations of coupled oscillators, *Phys. D*, **143** (2000), 1–20.
- [63] L. Timms and L.Q. English, Synchronization in phase-coupled Kuramoto oscillator networks with axonal delay and synaptic plasticity *Phys. Rev. E*, **89** (2014), 032906.
- [64] D.A. Wiley, S.H. Strogatz and M. Girvan, The size of the sync basin, *Chaos*, **16** (2006), 015103.
- [65] H.-M. Woo, Y. Hong, B. Kwon and B.-J. Yoon, Accelerating optimal experimental design for robust synchronization of uncertain Kuramoto oscillator model using machine learning, *IEEE Trans. Signal Process.*, **69** (2021), 6473–6487.
- [66] J. Wu and X. Li, Collective synchronization of Kuramoto-oscillator networks, *IEEE Circuits Syst. Mag.*, **20** (2020), 46–67.
- [67] K. Yagasaki, Bifurcations and stability of synchronized solutions in the Kuramoto model with uniformly spaced natural frequencies, *Nonlinearity*, **38** (2025), 075032; Corrigendum, **38** (2025), 109501.
- [68] K. Yagasaki, Continuum limit of the Kuramoto model with random natural frequencies on uniform graphs, *Phys. D*, **481** (2025), 134818.
- [69] K. Yagasaki, Bifurcations of synchronized solutions in a continuum limit of the Kuramoto model with two-mode interaction depending on two graphs, *SIAM J. Appl. Dyn. Syst.*, **24** (2025), 2345–2368.
- [70] K. Yagasaki, Bifurcations of twisted solutions in a continuum limit for the Kuramoto model on nearest neighbor graphs, submitted for publication.
- [71] K. Yagasaki, Feedback control of the Kuramoto model defined on uniform graphs I: Deterministic natural frequencies, submitted for publication. [arXiv:2505.02196 \[math.DS\]](https://arxiv.org/abs/2505.02196)
- [72] R. Yao, Y. Li, X. Yao, K. Wang, J. Qu, X. Zou and B. Hong, Brain wave dynamics in a Hopfield-Kuramoto model *Phys. Rev. E*, **111** (2025), 044310.
- [73] S. Zheng, Z. Liang, Y. Qu, Q. Wu, H. Wu and Q. Liu, Kuramoto model-based analysis reveals oxytocin effects on brain network dynamics, *Int. J. Neural Syst.*, **32** (2022), 2250002.
- [74] W. Zou, D.V. Senthilkumar, M. Zhan and J. Kurths, Quenching, aging, and reviving in coupled dynamical networks *Phys. Rep.*, **931** (2021), 1–72.

DEPARTMENT OF APPLIED MATHEMATICS AND PHYSICS, GRADUATE SCHOOL OF INFORMATICS,
KYOTO UNIVERSITY, YOSHIDA-HONMACHI, SAKYO-KU, KYOTO 606-8501, JAPAN

Email address: yagasaki@amp.i.kyoto-u.ac.jp